american physiological society
AMERICAN JOURNAL OF PHYSIOLOGY
RENAL PHYSIOLOGY

Am J Physiol Renal Physiol 321: F305–F321, 2021.
First published July 20, 2021; doi:10.1152/ajprenal.00081.2021

RESEARCH ARTICLE

Characterization of a functional V_{1B} vasopressin receptor in the male rat kidney: evidence for cross talk between V_{1B} and V_2 receptor signaling pathways

Annette Hus-Citharel,[1]* Nadine Bouby,[2]* Maithé Corbani,[3] Julie Mion,[3] Christiane Mendre,[3] Judit Darusi,[4] Csaba Tomboly,[4] Miguel Trueba,[5] Claudine Serradeil-Le Gal,[6] Catherine Llorens-Cortes,[1]* and Gilles Guillon[3]*

[1]*Collège de France, Neuropeptides Centraux et Régulations Hydrique et Cardiovasculaire, Centre Interdisciplinaire de Recherche en Biologie, Institut National de la Santé et de la Recherche Médicale, Centre National de la Recherche Scientifique, Paris, France;* [2]*Centre de Recherche des Cordeliers, Institut National de la Santé et de la Recherche Médicale, Sorbonne Université, Université de Paris, Paris, France;* [3]*Institut de Génomique Fonctionnelle, Institut National de la Santé et de la Recherche Médicale, Centre National de la Recherche Scientifique, Université de Montpellier, Montpellier, France;* [4]*Biological Research Center of the Hungarian Academy of Sciences, Szeged, Hungary;* [5]*Department of Biochemistry and Molecular Biology, Faculty of Science and Technology, Basque Country University, Leioa, Spain; and* [6]*Vibiosphen, Labège, France*

Abstract

Although vasopressin V_{1B} receptor ($V_{1B}R$) mRNA has been detected in the kidney, the precise renal localization as well as pharmacological and physiological properties of this receptor remain unknown. Using the selective V_{1B} agonist d[Leu^4, Lys^8]VP, either fluorescent or radioactive, we showed that $V_{1B}R$ is mainly present in principal cells of the inner medullary collecting duct (IMCD) in the male rat kidney. Protein and mRNA expression of $V_{1B}R$ were very low compared with the V_2 receptor (V_2R). On the microdissected IMCD, d[Leu^4, Lys^8]VP had no effect on cAMP production but induced a dose-dependent and saturable intracellular Ca^{2+} concentration increase mobilization with an EC_{50} value in the nanomolar range. This effect involved both intracellular Ca^{2+} mobilization and extracellular Ca^{2+} influx. The selective V_{1B} antagonist SSR149415 strongly reduced the ability of vasopressin to increase intracellular Ca^{2+} concentration but also cAMP, suggesting a cooperation between $V_{1B}R$ and V_2R in IMCD cells expressing both receptors. This cooperation arises from a cross talk between second messenger cascade involving PKC rather than receptor heterodimerization, as supported by potentiation of arginine vasopressin-stimulated cAMP production in human embryonic kidney-293 cells coexpressing the two receptor isoforms and negative results obtained by bioluminescence resonance energy transfer experiments. In vivo, only acute administration of high doses of V_{1B} agonist triggered significant diuretic effects, in contrast with injection of selective V_2 agonist. This study brings new data on the localization and signaling pathways of $V_{1B}R$ in the kidney, highlights a cross talk between $V_{1B}R$ and V_2R in the IMCD, and suggests that $V_{1B}R$ may counterbalance in some pathophysiological conditions the antidiuretic effect triggered by V_2R activation.

NEW & NOTEWORTHY Although $V_{1B}R$ mRNA has been detected in the kidney, the precise renal localization as well as pharmacological and physiological properties of this receptor remain unknown. Using original pharmaceutical tools, this study brings new data on the localization and signaling pathways of $V_{1B}R$, highlights a cross talk between $V_{1B}R$ and V_2 receptor (V_2R) in the inner medullary collecting duct, and suggests that $V_{1B}R$ may counterbalance in some pathophysiological conditions the antidiuretic effect triggered by V_2R activation.

calcium and cAMP signaling; diuresis; inner medullary collecting duct; receptor heterodimerization; vasopressin V_{1B} and V_2 receptors

INTRODUCTION

In mammals, the nonapeptide arginine vasopressin (AVP) synthesized in the hypothalamus is involved in multiple physiological effects including inhibition of diuresis, vasoconstriction of vascular smooth muscle cells, stimulation of hepatic glycogenolysis and adenocorticotropic hormone release, and modulation of social behavior in humans and rodents (1–4). The effects of AVP are mediated by stimulation of tissue-specific G protein-coupled receptors classified in two major types, V_1 and V_2, according to their transduction pathways. The vasopressin V_1 receptor (V_1R), later

* A. Hus-Citharel and N. Bouby contributed equally to this work. C. Llorens-Cortes and G. Guillon contributed equally to this work.
Correspondence: N. Bouby (nadine.bouby@inserm.fr); G. Guillon (gilles.guillon@igf.cnrs.fr).
Submitted 24 February 2021 / Revised 28 June 2021 / Accepted 19 July 2021

subdivided into V_{1A} and V_{1B} subtypes, mediates signaling through Ca^{2+} and diacylglycerol (DAG) transducer pathways (5, 6), whereas the vasopressin V_2 receptor (V_2R) signals mainly through cAMP (7, 8).

In addition to this classification, another type of vasopressin receptor, called "V_2-like," has been identified in different tissues, including the inner medullary collecting duct (IMCD) of the kidney (9–13). Stimulation of this atypical "V_2-like" receptor by the V_2R agonist 1-desamino-8-D-arginine vasopressin (dDAVP) induces an increase in the intracellular Ca^{2+} concentration ($[Ca^{2+}]_i$) in the IMCD, and this receptor isoform has been proposed to be $V_{1B}R$ (14). Indeed, $V_{1B}R$ mRNA has been detected in the renal medulla, and pharmacological characteristics of the V_2-like receptor in cultured cells of the rat IMCD were similar to that of human (h)$V_{1B}R$ expressed in Chinese hamster ovary cells (13, 14).

The IMCD plays a key role in the establishment of the corticomedullary osmolality gradient and urinary concentrating mechanism. Vasopressin binding to basolateral V_2R promotes insertion of aquaporin 2 (AQP2) into the luminal face of the collecting duct (CD) and increases water permeability. Yet, Han et al. (12) have demonstrated that vasopressin-stimulated $[Ca^{2+}]_i$ increases via V_1R may be responsible for a negative control of water reabsorption in IMCD tubules. Moreover, vasopressin, upon binding to V_2R, increases urea permeability through activation of urea transporter-A1 in the terminal part of the IMCD, thus allowing the delivery of concentrated urea to the renal papillary interstitium, a critical step in urine concentration (16, 17). Beside these functional effects, sustained elevated level of AVP concentration in vivo has been shown to stimulate proliferation of tubular cells expressing V_2R in the renal medulla (18). So far, the physiological role of $V_{1B}R$ in the kidney, especially in the IMCD, is yet to be determined. A role for $V_{1B}R$ in the body water balance was suggested by the higher water intake and daily urine volume observed in $V_{1B}R$ knockout mice compared with wild-type mice (19).

Thus, the present work was undertaken to *1*) determine the precise localization of $V_{1B}R$ mRNA and protein within the rat kidney, *2*) study on the freshly microdissected IMCD, the coupling of $V_{1B}R$ to second messenger cascades (cAMP production and intracellular Ca^{2+} mobilization), and *3*) attempt to elucidate the physiological role of $V_{1B}R$ in participating with V_2R to a fine regulation of vasopressin action at the kidney level.

MATERIAL AND METHODS

Drugs

Most standard chemicals were purchased from Sigma (St. Louis, MO), Roche Molecular Biochemicals (Mannheim, Germany), or Merck and Co. (Darmstadt, Germany) unless otherwise indicated. Bromodeoxyuridine (BrdU) and phorbol 12-myristat 13-acetate (PMA) were from Sigma (Lisle d'Abeau Chesne, France). Gö6976 was from Merck Chemistry (Fontenay-sous-Bois, France). AVP and dDAVP were from Bachem (Bubendorf, Switzerland). SSR49059, SSR121463B, SSR126768A, and SSR149415 were kindly provided by Sanofi (Toulouse, France). [^{3}H]AVP (60–80 Ci/mmol) and [^{3}H]adenine (27 Ci/mmol) were obtained from Perkin-Elmer Life Sciences (Courtaboeuf, France). Lipofectamine 2000 was from Invitrogen. cAMP measurements were performed with the Gs Dynamic kit from Cisbio Bioassays (Codolet, France). d(CH_2)$_5$[Tyr(Me)^2]AVP ("Manning compound"), d[Leu^4, Lys^8]VP, and d[Leu^4, Lys(Alexa647)^8]VP were synthesized and kindly provided by Dr. M. Manning (University of Toledo, Toledo, OH). [^{3}H]d[Leu^4, Lys^8]VP (87.8 Ci/mmol) was synthetized by Dr. C. Tomboly (Biological Research Center, Szeged, Hungary) and characterized by our group (see Ref. 20 and the present study). AQP2 rabbit polyclonal antibody (Cat. No. SC-9882, lot 1295) was from Santa Cruz Biotechnologies (Dallas, TX). Mouse monoclonal anti-BrdU antibody (BU33-CatB8434) was from Sigma. Cy3-labeled secondary goat antirabbit antibody (Cat. No. 711-160-132) and Cy3-labeled secondary donkey antimouse antibody (Cat. No. 715-167-003) were from Jackson ImmunoResearch (Interchim, Monluçon, France).

Animals

Male Sprague-Dawley rats (200–250 g, Janvier, Le Genest-St-Isle, France) were housed in light (12-h dark and 12-h light)- and temperature (21°C)-controlled rooms and had free access to standard dry food and tap water. All procedures in this study conformed with animal welfare guidelines of the European Community and were approved by the local ethical committee (Authorization No. 34.128 for experimentation).

Binding Assay on Plasma Membranes

Membrane preparation and incubation with radioligands such as [^{3}H]AVP or [^{3}H]d[Leu^4,Lys^8]VP were performed, as previously described (20). Briefly, rats were euthanized by cervical dislocation and decapitated, and the kidneys were quickly removed and placed in ice-cold homogenization buffer. Crude plasma membranes were prepared from the inner medulla (IM) and used immediately for binding experiments. For saturation binding experiments, 10–100 μg of membrane protein were incubated for 60 min at 37°C in 200 μL of medium containing 50 mmol/L Tris-HCl (pH 7.4), 3 mmol/L $MgCl_2$, 1 mg/mL BSA, 0.01 mg/mL leupeptin, and increasing concentrations (0.5–15 nmol/L) of tritiated hormone with (nonspecific binding) or without (total binding) 0.1 μmol/L unlabeled AVP. For competition experiments, membrane proteins were incubated as described above with 1 nmol/L of [^{3}H]AVP or [^{3}H]d[Leu^4, Lys^8]VP and increasing amounts of the $V_{1B}R$ antagonist SSR149415. Plasma membrane-associated radioactivity was collected by filtration through GF/C filters and counted. Specific binding was calculated in each condition as the difference between total and nonspecific binding. Data were analyzed by GraphPad PrismTM (GraphPad Software, San Diego, CA). K_d and maximal binding capacity (B_{max}) were deduced from Scatchard experiments, and K_i was determined from competition experiments.

To validate the new radioactive probe [^{3}H]d[Leu^4, Lys^8]VP, crude plasma membranes from rat tissues such as the liver or kidney naturally expressing vasopressin V_{1A} receptor ($V_{1A}R$) or V_2R, respectively, were challenged. Membranes from transiently transfected Chinese hamster ovary or AtT20 cells expressing rat oxytocin receptor (OTR) or $V_{1B}R$

were also used, as previously described (20). The results showed that [^{3}H]d[Leu^4, Lys^8]VP exhibited a very good affinity (0.36 nmol/L) for rat V_{1B}R and a relatively good selectivity versus the other rat vasopressin receptor isoforms (K_d of 25.6 nmol/L for V_{1A}R, 5.7 nmol/L for V_2R, and 5.6 nmol/L for OTR). This selectivity was better than that of [^{3}H]AVP, which displayed a similar K_d value for all receptor types (1.5 nmol/L for V_{1A}R, 0.7 nmol/L for V_2R, 0.9 nmol/L for OTR, and 3.4 nmol/L for V_{1B}R) (21). Moreover, the high-specific radioactivity (87.8 Ci/mmol) of [^{3}H]d[Leu^4, Lys^8]VP allowed detection of low amounts of V_{1B}R binding sites.

Labeling and Imaging Rat Kidney Slices Using V_{1B}R Fluorescent Analog

Rats were euthanized, and the kidneys were immediately immersed in sectioning buffer (21) and sectioned in 350-μm-thick slices at 2°C in sagittal orientation. The labeling protocol was as previously published (22). Briefly, slices were collected and incubated in 12-well plates first for 30 min at 12°C in 1 mL DMEM, 0.2 mg/mL BSA, and 25 mmol/L HEPES buffer (pH 7.4) containing 250 nmol/L of Manning compound to prevent any V_{1A}R/OTR detection, and then for 1 h with 150 nmol/L d[Leu^4, Lys(Alexa647)^8]VP and in the presence of the same V_{1A}R/OTR antagonist. Nonspecific binding was evaluated on adjacent slices by displacement in the presence of an excess (1 μmol/L) of AVP. Slices were washed three times with 1.4 mL PBS on ice, and 4% paraformaldehyde was added for overnight fixation at 4°C. After two new washes, antibodies were added at the relevant dilution in PBS-2 mg/mL BSA-0.2% Triton X-100 (1 mL/slice), and the 12-well plate was incubated overnight at 4°C. To localize principal cells of the kidney tubule, rabbit polyclonal AQP2 antibody was used at a final dilution of 1/1,000 (overnight at 4°C). The next day, after three washes (1.4 mL PBS), Cy3-labeled secondary antibody goat antirabbit (1/2,000) was added in the same PBS-BSA-Triton X-100 buffer, and slices were incubated for 1 h at room temperature with gentle rocking. After three washes, 0.5 μL Hoechst in 1 mL PBS was added, incubated at least for 15 min, and rinsed. Slices were kept in 0.2% sodium azide at 4°C before being imaged. Imaging was performed with a macroconfocal wide field LSI Leica microscope using a ×5 air objective. Slices were mounted in chambers consisting of glass slides equipped with spacers finally covered with a coverslip and filled with PBS at room temperature. Three lasers were used: diode 405 (Hoescht) for detecting nuclei and helium/neon 561 nm (Cy3) for AQP2 and helium 633 for Alexa647-labeled V_{1B}R ligand bound to receptors with the corresponding window settings for collecting emissions. Overlapping was avoided by correct and exclusive adjustment of the emission windows. Images (.lif) were converted by the Leica software in .tif and mounted using Photoshop.

Microdissection of Nephron Segments

The left kidney of male Sprague–Dawley rats (body weight: 150 g) was prepared for microdissection of the nephron, as previously described (23). Pieces of the CD were isolated under stereomicroscopic observation from the cortex (CCD), outer medulla (OMCD), and inner medulla (IMCD). Afferent arterioles were isolated with the glomerulus and identified according to their morphology, as previously described (24). Microdissected segments (3–13 segments) were obtained from three to eight rats for each mean experimental value.

Quantification of mRNA Expression Levels by Real-Time RT-PCR

Approximately 20-mm tubular lengths were used for total RNA extraction. Total RNAs were extracted using TRIzol LS reagent (Invitrogen, Basel, Switzerland), according to the manufacturer's instructions. RNA (1 μg) was first reverse transcribed using Superscript III reverse transcriptase (Invitrogen) and 250 ng of random hexamer (Amersham Biosciences Europe, Orsay, France) at a final volume of 20 μL. Real-time PCRs were performed using SYBR Green PCR Master Mix (Applied Biosystems, Foster City, CA) with 1:10 of the reverse transcription product and carried out on an ABI 7500 Sequence Detector (Applied Biosystems). The sequences of the primers used (concentration: 300 nmol/L) were 5′-CCAATGAAGATTCTACCAATGTG-3′ (forward) and 5′-ATGGTGGCTCAAGGAACG-3′ (reverse) for *Avpr1b* mRNA, 5′-GTGCCATCTGCCGCCCTAT-3′ (forward) and 5′-CCCACTGCCATTTCCCACATC-3′ (reverse) for *Avpr2* mRNA, and finally 5′-ATGATTCTACCCACGGCAAG-3′ (forward) and 5′-CTGGAAGATGGTGATGGGTT-3′ (reverse) for *Gapdh* mRNA, which was used as an internal control. After an initial denaturation step of 10 min at 95°C, the thermal cycling conditions were 40 cycles at 95°C for 15 s and 60°C for 1 min. Each sample was tested in triplicate. Data were normalized to the expression levels of GAPDH mRNA.

$[Ca^{2+}]_i$ Measurement

Experiments were performed as previously described (25). Briefly, microdissected nephron segments and glomerular arterioles were loaded with 5 μmol/L Fura-2 AM at room temperature for 120 min. Each nephron segment or arteriole was continuously superfused at 37°C with either medium or the solutions to be tested. The V_{1B}-selective agonist (d[Leu^4, Lys^8]VP) and V_2-selective agonist (dDAVP) were applied for 5 min. For experiments performed in the absence of external Ca^{2+}, IMCDs were superfused in Ca^{2+}-free medium 2 min before addition of the agonist. For experiments with specific antagonists, CDs were superfused for 15 min before addition of the agonist. The Ca^{2+} response was evaluated by determining the magnitude of the response ($\Delta[Ca^{2+}]_i$) corresponding to the difference between peak and basal concentrations (in nmol/L) or by determining the area under the curve (in nmol·s/L) obtained by the integral of the Ca^{2+} signal.

Intracellular cAMP Measurement in the Microdissected IMCD

cAMP levels were measured in the microdissected IMCD using the Gs Dynamic2 kit based on homogeneous time-resolved fluorescence technology. The method is a competitive immunoassay between native cAMP produced by cells of the CD and cAMP labeled with *dye 2*. The tracer binding was visualized by Mab anti-cAMP labeled with cryptate. Results are expressed as fmoles of cAMP produced per 0.4-mm tubular length and per 10-min incubation time at 37°C.

Measurement of cAMP Accumulation in Human Embryonic Kidney-293 Cells Coexpressing $V_{1B}R$ and/or V_2R

Human embryonic kidney (HEK)-293 cells were seeded in 96-well plates precoated with polyornithine at a density of 30,000 cells/well and transfected with $V_{1B}R$ and/or V_2R plasmids using Lipofectamine 2000, according to the manufacturer. DNA constructs were generated by PCR amplification using full-length human wild-type $V_{1B}R$ (26) and V_2R (kindly provided by D. Devost and M. Bouvier, Montreal University, Montreal, QC, Canada), as previously described. Forty-eight hours after transfection, cells were pretreated with PMA (15 min, 1 μmol/L) and/or Gö6976 (30 min, 100 nmol/L) and then treated for 30 min at 37°C with or without AVP in the presence of phosphodiesterase (PDE) inhibitor [RO201724 (0.1 mmol/L)]. The cAMP produced was detected using the homogeneous time-resolved fluorescence Gs Bioassay (Dynamic 2 kit, CisBio). Plates were read on a PHERAstar FS (BMG Labtech, Champigny, France). The specific fluorescence resonance energy transfer signal was calculated using the following equation: $\Delta F\% = 100 \times (R_{pos} - R_{neg})/(R_{neg})$, where R_{pos} is the fluorescence ratio (665/620 nm) calculated in wells incubated with both donor-labeled antibody and acceptor d2 and R_{neg} is the same ratio for the negative control incubated only with the donor fluorophore-labeled antibody. The fluorescence resonance energy transfer signal (ΔF %), inversely proportional to the quantity of cAMP, was then transformed into cAMP concentration using a calibration curve prepared on the same plate.

Bioluminescence Resonance Energy Transfer Assay

$V_{1A}R$, V_2R, and OTR hybrid constructs were generated from human receptors subcloned in PRK5 vector using the GeneEditor In Vitro Site-Directed Mutagenesis System (Promega, Madison, WI), as previously described by Terrillon et al. (27) (gift from Dr. Devost and M. Bouvier). hV_{1B} and $hV_{1B}RL$ were cloned in pRL-CMV and pcDNA3.0 vectors, respectively, whereas corticotropin-releasing factor 1 (CRF1)-enhanced yellow fluorescent protein (EYFP) was in pEYFP-N1 (Clontech) and $GABA_{B2}$ receptor-enhanced green fluorescent protein (EGFP) was in pcDNA3.0, according to the constructions used in our previous work (26). All vectors contained similar cytomegalovirus promotor and simian virus 40 polyadenylation sites for comparable expression levels. Mild levels of receptor expression were chosen in these experiments to mimick physiological conditions [<1 pmol/mg protein (26)]. Bioluminescence resonance energy transfer (BRET) experiments were conducted, as previously described (26). Briefly, wild-type $hV_{1B}R$, $hV_{1B}RL$, and/or hV_2-EYFP receptors were transiently transfected in HEK-293 cells using the Jet PEI technique with a constant amount of the donor construct ($hV_{1B}RL$, 1 μg of DNA) and from 0.03 to 10 μg of acceptor (hCRF1-EYFP, hV_2-EYFP, or $hGABA_{B2}$-EYFP) DNA constructs in 96-well plates, with each well seeded with 20,000 cells. For BRET competition, hV_2RLuc and hV_2-EYFP were cotransfected at the same concentration of 1 μg each, and wild-type untagged receptors ($hV_{1A}R$, $hV_{1B}R$, or hOTR) were added at increasing concentrations. Two days after transfection, HEK-293 cells were washed twice in HBS medium with 5.55 mmol/L glucose and further incubated in the same medium supplemented with 2.5 μmol/L coelenterazine h substrate (Promega) at a total volume of 50 μL/well at 30°C. BRET reading was performed immediately using the Mithras LB 940 plate reader (Berthod Biotechnologies, Oak Ridge, TN), allowing the integration of the short wavelength filter (440 – 500 nm) and long wavelength filter (510–590 nm). Background values obtained with mock-transfected HEK-293 cells were subtracted in total luminescence and in fluorescence measurements, and mean values of triplicate wells/sample were calculated. BRET signals were calculated and expressed in milli BRET units of the BRET ratio.

Urine Flow Measurement

The effects of agonist or antagonist on diuresis were tested in a separate series of male Sprague–Dawley rats. Rats were individually housed in metabolic cages with free access to tap water and powdered food. After 3–5 days of habituation, they were divided into groups of equivalent urine volume and osmolality. In *experiment I*, rats received an intraperitoneal injection of vehicle (saline) or a low (0.42 μg/kg) or high dose (72 μg/kg) of $V_{1B}R$ agonist d[Leu^4, Lys^8]VP) (n = 5 rats/group). In *experiment II*, rats received by oral route either vehicle (2 mL/kg in 5% DMSO, 5% cremophor EL, or 90% saline) or V_{1B} antagonist SSR149415 (30 mg/kg) (n = 6 rats/group). Vehicle or drug was administrated at 10 AM. Urine was collected for 5–6 h starting just after the injection. Urine volume was determined gravimetrically, assuming the density of urine was equal to unity. Urine osmolality was measured using a freezing point osmometer (Roebling). A similar experiment was performed in rats pretreated with AVP (400 ng/day infused intraperitoneally for 5 days with Alzet minipumps) inducing a 300% increase of plasmatic AVP (18), which is in the physiological range of plasma concentration of this hormone.

In Vivo Measurement of Renal Proliferation Upon Vasopressin Analog Administration

Male Sprague-Dawley rats were subcutaneously implanted for 3 days with osmotic minipumps (model 2001, Alzet, Charles River, France) delivering d[Leu^4, Lys^8]VP (40 μg/kg·day), dDAVP (2 μg/kg·day), or PBS alone. In vivo cell proliferation experiments were performed using BrdU incorporation, as previously described (18). Labeled nuclei were numbered on four sections of different renal zones and four animals per experimental group. Data were statistically compared using the nonparametric test of Mann–Whitney.

Data Analysis

Results are expressed as means ± SE. For experiments on $[Ca^{2+}]_i$ or cAMP, the number of segments is indicated in the figures. Statistical differences were assessed using a paired t test taking into account values obtained before the addition of the agonist (basal level) and those obtained after stimulation with the agonist (peak value) or one-way ANOVA on weighted means followed by Fisher's test.

RESULTS

Evidence of V_{1B} mRNA and Receptor Binding Sites in the IM

V_{1B}R and V_2R mRNAs were quantified by real-time RT-PCR in three parts of the CD: the CCD, OMCD, and IMCD (Fig. 1*A*). The highest V_{1B}R mRNA expression was found in the IMCD, whereas weak expression was detected in the CCD and OMCD. V_2R mRNA was present in all segments and was 211-fold more abundant than V_{1B}R mRNA in the IMCD.

Localization of V_{1B}R protein within the rat kidney was studied using the selective fluorescent V_{1B} analog d[Leu^4, Lys(Alexa647)^8] VP (150 nmol/L), which exhibit a high fluorescence brightness in the far red spectrum area where autofluorescence of the tissue is low (20). A discreet but reproducible labeling was observed only in the IM. This labeling was specific as it completely disappeared when incubation with the fluorescent probe was performed in the presence of an excess of unlabeled AVP (1 µmol/L; Fig. 1*B*). Numerous cells exhibiting V_{1B}R-specific staining (74 ± 6%, n = 30 cells from 3 distinct preparations) were also immunoreactive for anti-AQP2 antibody (Fig. 1*B*, *bottom*). As it is well known that AQP2 and V_2R are expressed in principal cells of the renal CD (28), this strongly suggests that V_{1B}R was colocalized with V_2R in IMCD cells, but the scattering of the fluorescent signal prevented precise determination of the apical or basolateral location of the receptor.

Pharmacological Characterization of V_{1B}R in Plasma Membranes of the IM

A radioligand binding assay with [^{3}H]d[Leu^4, Lys^8]VP was used to quantify V_{1B}R density in plasma membranes from the IM. The specific binding of [^{3}H]d[Leu^4, Lys^8]VP was dose dependent and saturable (Fig. 2*A*), as observed for [^{3}H]AVP

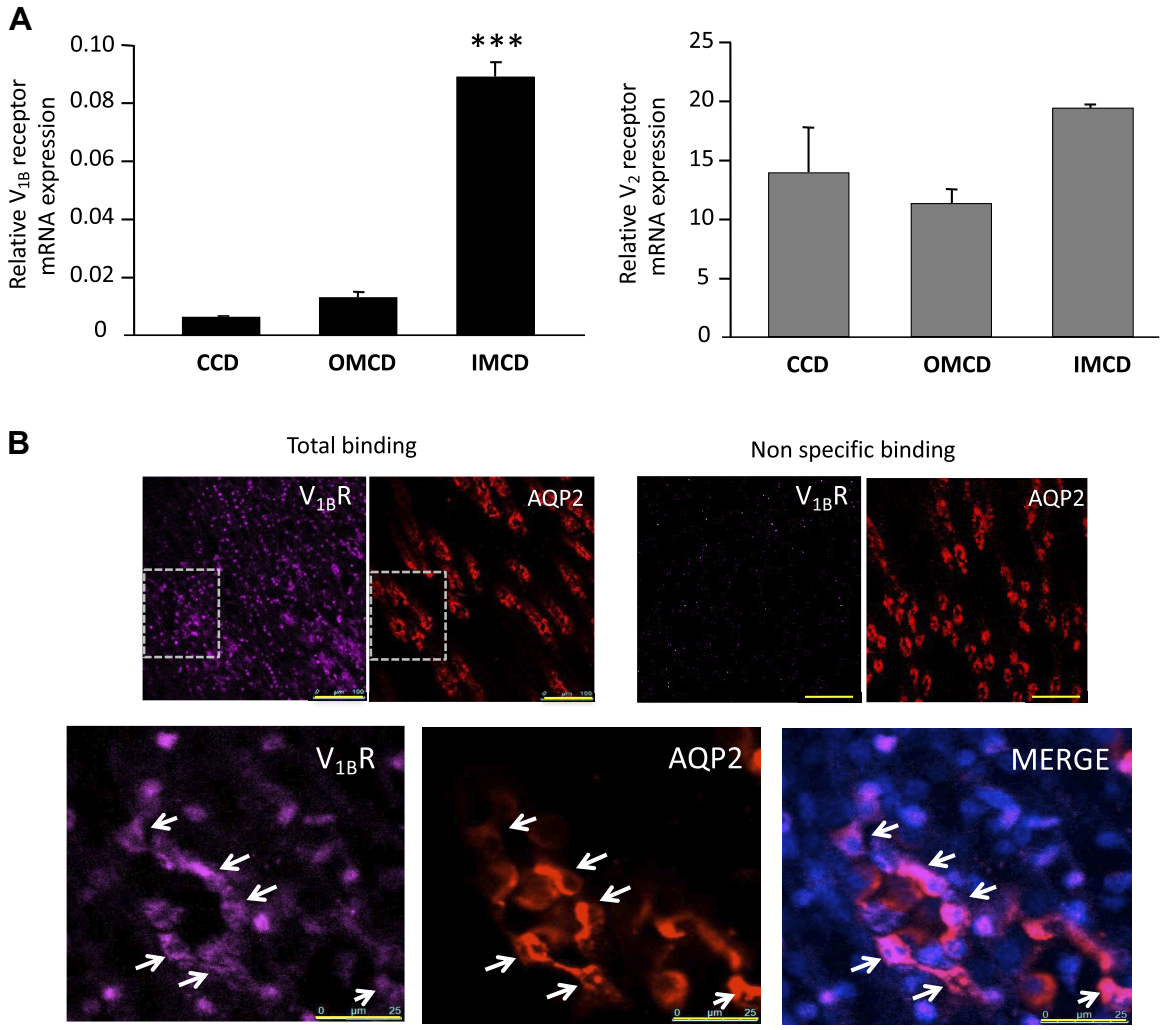

Figure 1. Distribution of mRNA and vasopressin V_{1B} receptor (V_{1B}R) within the kidney. *A*: expression of V_{1B}R and vasopressin V_2 receptor (V_2R) mRNA in the cortical collecting duct (CCD), outer medullary collecting duct (OMCD), and inner medullary collecting duct (IMCD). Results are expressed as the relative value from 2-mm tubular length normalized with the housekeeping gene GAPDH. Each histogram represents means data ± SE in the CCD (n = 3 rats) and OMCD (n = 3 rats) and IMCD (n = 6 rats). ***$P < 0.0001$ vs. the CCD and OMCD. *B*: colocalization of V_{1B}R and V_2R in the inner medulla. *Top*: representative confocal images of rat kidney slices incubated with the fluorescent V_{1B} analog d[Leu^4(Lys-Alexa647)^8]VP (purple) or aquaporin 2 (AQP2) antibody (red) in the presence (nonspecific binding) or absence (total binding) of 1 µmol/L of unlabeled arginine vasopressin (AVP). Scale bar = 100 µm. *Bottom*: zoomed images of the inner medulla, showing that V_{1B}R and AQP2 are colocalized in the same cells (merge, arrows). Scale bar = 25 µm.

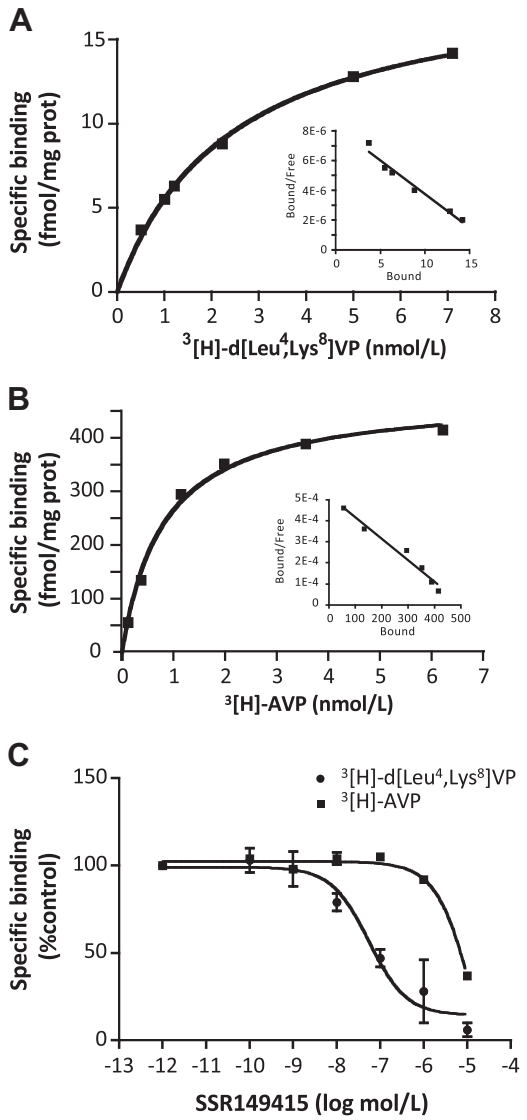

Figure 2. Pharmacological characterization of rat vasopressin V_{1B} receptor in the kidney using a selective tritiated probe. Crude plasma membranes from the inner medulla of the rat kidney were incubated for 1 h at 37°C with either increasing amounts of [^{3}H]d[Leu^4, Lys^8]VP (100 µg protein/assay) (*A*), or [^{3}H]arginine vasopressin (AVP; 10 µg protein/assay) (*B*), with or without 100 nmol/L of unlabeled AVP. Specific binding was calculated in each experimental condition, and Scatchard representation of dose-dependent binding curves is shown. Results are means ± SE of three independent experiments, each in triplicate. *C*: binding displacement of [^{3}H]AVP or [^{3}H]d[Leu^4, Lys^8]VP with the selective V_{1B} antagonist SSR149415. Experiments were performed as described in *A* and *B* with either 0.5 nmol/L [^{3}H]AVP or 1.5 nmol/L [^{3}H]d[Leu^4, Lys^8]VP and with or without (control) increasing amounts of SSR149415. Specific binding calculated in each experimental condition is expressed as the percentage of control specific binding and is the means ± SE of three distinct experiments each performed in triplicate.

binding on plasma membranes from the IMCD (Fig. 2*B*). The Scatchard representation indicated the presence of a single class of binding sites exhibiting a nanomolar affinity (K_d = 2.1 ± 0.3 nmol/L) and a low B_{max} value (B_{max} = 19 ± 5 fmol/mg protein) for [^{3}H]d[Leu^4, Lys^8]VP. By comparison, experiments performed on the same membrane preparation with [^{3}H]AVP that binds to all vasopressin receptor isoforms gave a K_d value of 0.7 ± 0.1 nmol/L and a B_{max} value of 493 ± 62 fmol/mg protein. The binding selectivity of the radioligand [^{3}H]d[Leu^4, Lys^8]VP was further confirmed in heterologous displacement experiments. The V_{1B}R-specific antagonist SSR149415 effectively displaced [^{3}H]d[Leu^4, Lys^8]VP with a rather good affinity (K_i = 29 ± 14 nmol/L), whereas it competed for the [^{3}H]AVP binding sites with a much lower affinity (K_i = 6,400 ± 900 nmol/L; Fig. 2*C*).

Effect of d[Leu^4, Lys^8]VP on Intracellular Ca^{2+} Mobilization Along the CD

The $[Ca^{2+}]_i$ response to the V_{1B}-selective agonist d[Leu^4, Lys^8]VP was tested in the CCD, OMCD, and IMCD. In good agreement with the distribution of V_{1B}R mRNA, 10 nmol/L d[Leu^4, Lys^8]VP elicited a significant $[Ca^{2+}]_i$ response only in the IMCD (Fig. 3*A*) and not in the OMCD (Fig. 3*B*) or in the CCD (Fig. 3*C*), whereas AVP induced a strong $[Ca^{2+}]_i$ response in all segments. The Ca^{2+} response induced by d[Leu^4, Lys^8]VP in the IMCD was rapid and reversible (Fig. 3*A*). This effect was dose dependent, discreet, but robust, with an EC_{50} value of 19 ± 6 nmol/L (Fig. 3*D*). The increase in $[Ca^{2+}]_i$ was maximal with 100 nmol/L d[Leu^4, Lys^8]VP with a maximal efficacy (E_{max}) of 108 ± 22 nmol/L (n = 8). The Ca^{2+} response induced by AVP in this nephron segment was not affected by a first application of 100 nmol/L V_{1B} agonist [$\Delta[Ca^{2+}]_i$: 343 ± 57 (n = 8) and 339 ± 45 nmol/L (n = 14) without and with preapplication, respectively].

As V_2R present in the IMCD also elicits $[Ca^{2+}]_i$ increases (25), we compared the Ca^{2+} response induced by d[Leu^4, Lys^8]VP with that induced by the selective V_2 agonist dDAVP. Both selective agonists (V_{1B} and V_2, respectively) exhibited a saturable dose-dependent response (Fig. 3*D*). dDAVP was more efficient at a low dose, which was in good agreement with its higher binding affinity for V_2R. Interestingly, both V_{1B} and V_2 agonists induced the same maximal response, 2.5 times lower than that obtained with the natural hormone AVP (100 nmol/L; Fig. 3*E*). We also investigated whether the responses induced by inframaximal doses of d[Leu^4, Lys^8]VP (10 nmol/L) or dDAVP (1 nmol/L) were additive. As shown in Fig. 3*F*, simultaneous application of the two agonists at these concentrations elicited additive effects.

To evaluate the relative importance of the intracellular Ca^{2+} release and/or external Ca^{2+} influx induced by d[Leu^4, Lys^8]VP, we compared the results obtained in the presence or absence of external Ca^{2+}. As shown in Fig. 4*A*, the peak phase induced by 10 nmol/L d[Leu^4, Lys^8]VP was attenuated and returned quickly to the basal level in the absence of external Ca^{2+}. By comparing the integral of the Ca^{2+} responses obtained with and without 2 mmol/L of external Ca^{2+}, it was possible to calculate the relative part of the intracellular Ca^{2+} mobilization and Ca^{2+} influx. As shown in Fig. 4*B*, activating V_{1B}R mainly triggered Ca^{2+} influx (~70% of the global Ca^{2+} response) rather than the release from intracellular pools. In contrast, an opposite profile was obtained using dDAVP, where influx and Ca^{2+} release participated equally to the global Ca^{2+} response (Fig. 4, *C* and *D*).

Specificity of the $[Ca^{2+}]_i$ Response Induced by d[Leu^4, Lys^8]VP in the IMCD

To confirm the respective contribution of V_{1B}R and V_2R to AVP-stimulated Ca^{2+} mobilization, we performed experiments

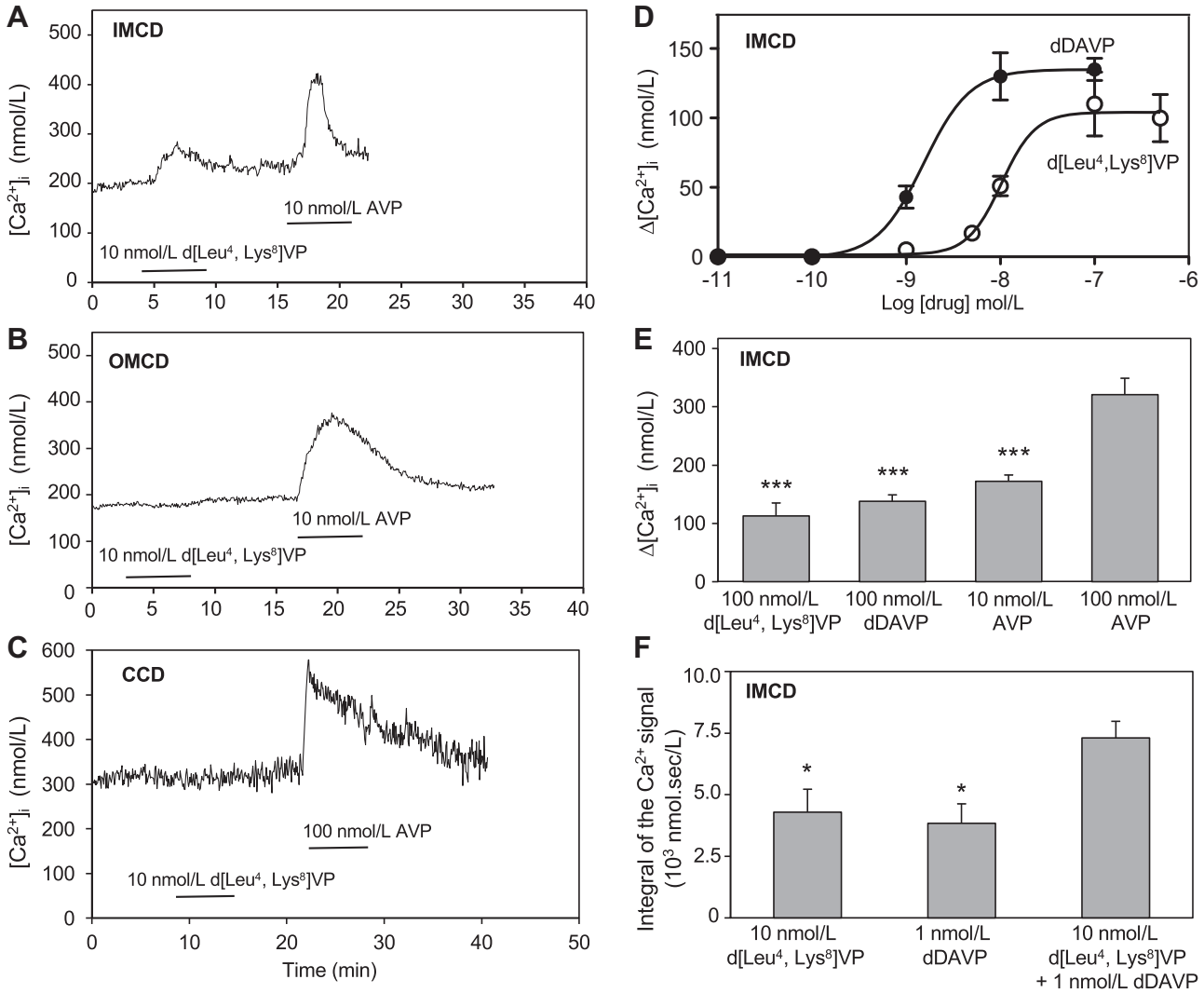

Figure 3. Effect of vasopressin agonists on intracellular Ca^{2+} mobilization along the collecting duct. *A*–*C*: representative recordings of intracellular Ca^{2+} concentration ($[Ca^{2+}]_i$) levels elicited by 10 nmol/L d[Leu^4, Lys^8]VP and, as controls, 10–100 nmol/L arginine vasopressin (AVP) in the inner medullary collecting duct (IMCD), outer medullary collecting duct (OMCD), and cortical collecting duct (CCD). *D*: dose-dependency curve of d[Leu^4, Lys^8]VP and 1-desamino-8-D-arginine vasopressin (dDAVP)-induced $[Ca^{2+}]_i$ responses in the IMCD. Each point represents the means ± SE of at least three independent determinations. *E*: comparison of maximal $[Ca^{2+}]_i$ levels elicited by maximal doses of the V_{1B} agonist d[Leu^4, Lys^8]VP, of the selective V_2 agonist dDAVP, or of 10 or 100 nmol/L AVP in the IMCD. Each bar represents the means ± SE of at least seven independent determinations. ***$P < 0.001$ compared with 100 nmol/L AVP. *F*: additive effects of d[Leu^4, Lys^8]VP and dDAVP on $[Ca^{2+}]_i$ levels in the IMCD. Experiments were performed with non-saturating concentrations of agonist (10 nmol/L for d[Leu^4, Lys^8]VP and 1 nmol/L for dDAVP). Each bar represents the means ± SE of at least seven independent determinations. *$P < 0.05$ compared with d[Leu^4, Lys^8]VP + dDAVP.

with selective AVP and OTR antagonists. The effect of 10 nmol/L d[Leu^4, Lys^8]VP on $[Ca^{2+}]_i$ responses was totally abolished by a 15-min pretreatment with 100 nmol/L of the selective V_{1B} antagonist SSR149415 and could be restored after a wash (Fig. 5*A*), whereas this antagonist had no effect on the $[Ca^{2+}]_i$ response induced by the V_2 agonist dDAVP (Fig. 5*B*). Pretreatment with the specific V_2 antagonist SSR121463B totally blocked the $[Ca^{2+}]_i$ response to dDAVP, whereas carbachol, used as a control for cell viability, induced a clear Ca^{2+} response (Fig. 5*C*).

Considering the effect of the V_{1B}-specific agonist d[Leu^4, Lys^8]VP in the IMCD, pretreatments with specific V_2, V_{1A}, or OT antagonists (10 nmol/L SSR121463B, 100 nmol/L SSR49059, or 100 nmol/L SSR126768A, respectively) did not significantly affect the $[Ca^{2+}]_i$ response to d[Leu^4, Lys^8]VP [basal: 73 ± 19 nmol/L (n = 4) vs. 38 ± 5 nmol/L (n = 6) or vs. 45 ± 3 nmol/L (n = 3) or vs. 52 ± 6 nmol/L (n = 14), respectively; Fig. 5, *D*–*F*]. This indicates that V_2R, V_{1A}R, or OTR do not contribute to d[Leu^4, Lys^8]VP-induced Ca^{2+} activation.

The pharmacological selectivity of d[Leu^4, Lys^8]VP was further verified on two other freshly microdissected renal structures using a Ca^{2+} mobilization assay. In glomerular afferent arterioles known to express only V_{1A}R localized on vascular smooth muscle cells (29), 10 nmol/L d[Leu^4, Lys^8]VP did not induce any significant response (Fig. 5*G*). In contrast, the Ca^{2+} response induced by AVP was fully antagonized by pretreatment with the selective V_{1A} antagonist SSR49059 (Fig. 5*H*). In the OMCD that expresses V_2R and V_{1A}R (1) but not V_{1B}R, d[Leu^4, Lys^8]VP had no significant effect on $[Ca^{2+}]_i$, whereas 10 nmol/L dDAVP induced a marked response (Fig. 5*I*). This

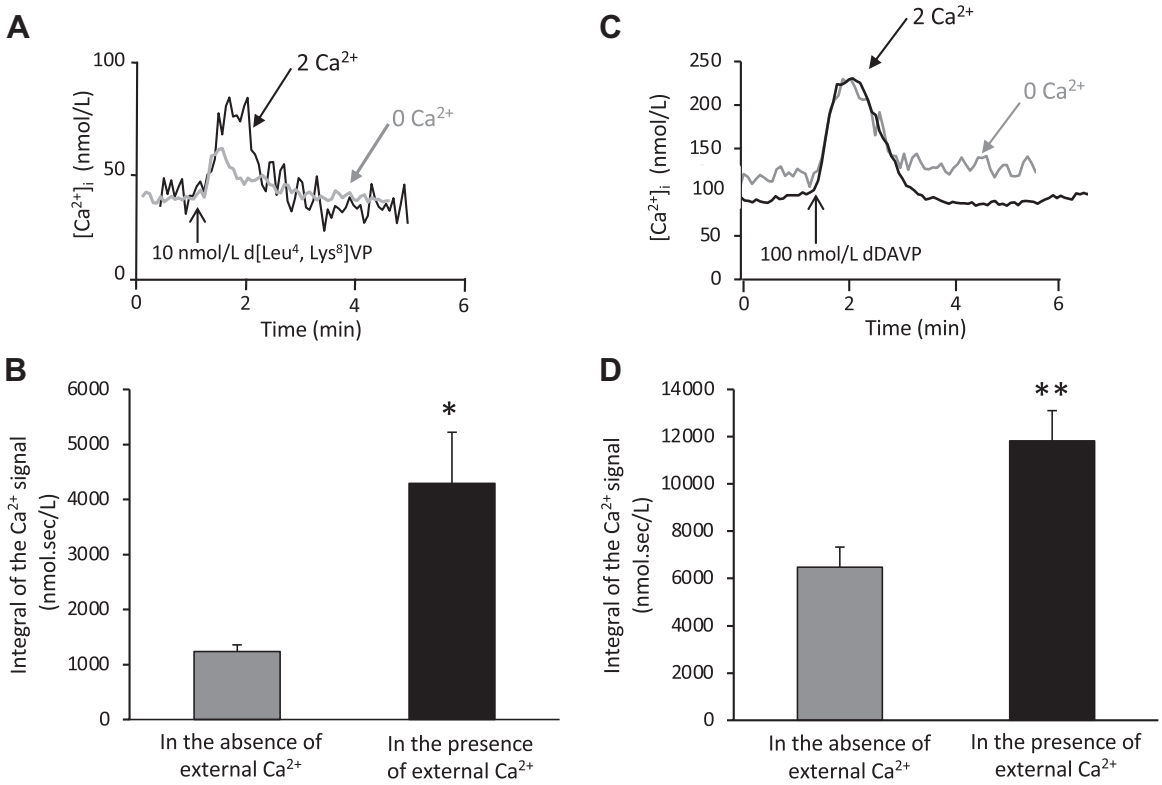

Figure 4. Influence of extracellular Ca^{2+} concentration on intracellular Ca^{2+} mobilization induced by d[Leu^4, Lys^8]VP or 1-desamino-8-D-arginine vasopressin (dDAVP) in inner medullary collecting duct. Experiments using 10 nmol/L d[Leu^4, Lys^8]VP or dDAVP were performed in the absence or presence of 2 mmol/L extracellular Ca^{2+}. *A* and *C*: representative traces of intracellular Ca^{2+} concentration ($[Ca^{2+}]_i$) obtained with either d[Leu^4, Lys^8]VP or dDAVP in the presence or absence of extracellular Ca^{2+}. *B* and *D*: histograms for Ca^{2+} release and Ca^{2+} influx elicited by d[Leu^4, Lys^8]VP or dDAVP. Results were calculated from traces as shown in *A* and *C*, respectively. Each result represents the integral of the Ca^{2+} signal calculated from five independent determinations. $^{**}P < 0.01$. $^{*}P < 0.05$.

effect of dDAVP was fully abolished by pretreatment with 10 nmol/L of the specific V_2 antagonist SSR121463B. The cell viability of the structures was verified by subsequent application of angiotensin II (Fig. 5*J*), which promoted the expected Ca^{2+} mobilization. These data demonstrate the specificity of the V_{1B} and V_2 agonists both used at 10 nmol/L in this study.

Effect of d[Leu^4, Lys^8]VP on cAMP Accumulation in the IMCD

As shown in Fig. 6*A*, d[Leu^4, Lys^8]VP did not significantly stimulate cAMP production even at the concentration of 100 nmol/L, a value allowing an almost complete occupation of V_{1B}R (Fig. 2*A*). In contrast, saturating doses of dDAVP (10 nmol/L) or AVP (50 nmol/L) induced robust and significant cAMP production (3.4-fold and 6.4-fold stimulation over the basal level, respectively).

By combining 10 nmol/L d[Leu^4, Lys^8]VP (a dose inducing 45% of maximal V_{1B}R occupancy and ineffective to stimulate cAMP) with 0.1 nmol/L dDAVP (a dose inducing 26% of maximal V_2R occupancy) (30), we observed a weak increase in dDAVP-induced cAMP production, but this effect remained not significant (Fig. 6*B*).

Effect of SSR149415 on cAMP Production and Intracellular Ca^{2+} Mobilization Induced by AVP in the IMCD

To elucidate the potential role of V_{1B}R on the overall response of the natural hormone AVP, we also evaluated the effect of a selective V_{1B} antagonist on signaling responses induced by AVP. As shown in Fig. 7, *A* and *B*, 100 nmol/L of SSR149415, which had no effect on the basal level of $[Ca^{2+}]_i$ and cAMP, reduced by 38% and 72% the maximal AVP-stimulated effect on $[Ca^{2+}]_i$ and cAMP production, respectively. This suggests a possible synergism between V_{1B}R and V_2R during AVP stimulation, as V_{1B}R activation by d[Leu^4, Lys^8]VP did not increase the cAMP level by itself (Fig. 6*A*). As controls, we performed similar experiments using 10 nmol/L dDAVP. Preincubation with 100 nmol/L SSR149415 had no effect on either the dDAVP-stimulated $[Ca^{2+}]_i$ increase (Fig. 5*B*) or dDAVP-stimulated cAMP production (111 ± 17 fmol/0.4 mm in the absence vs. 99 ± 17 fmol/0.4 mm in the presence of V_{1B} antagonist, n = 4 or 5 independent determinations).

V_{1B}R and V_2R Synergism Evaluated in HEK-293 Cells

To decipher which mechanism was involved in V_{1B}R/V_2R synergism, we performed experiments on HEK-293 cells on which we may manipulate the relative amounts of hV_{1B} and hV_2R by transfection. We decided to use hV_{1B}R and hV_2R since *1*) the tagged versions of these two human vasopressin receptors have been previously generated and pharmacologically validated in the laboratory (26) and *2*) compared with rat vasopressin receptors, hV_{1B}R and hV_2R exhibit very similar pharmacological properties and high sequence homologies in the intracellular loops that are involved in G protein coupling and to second messenger production (31).

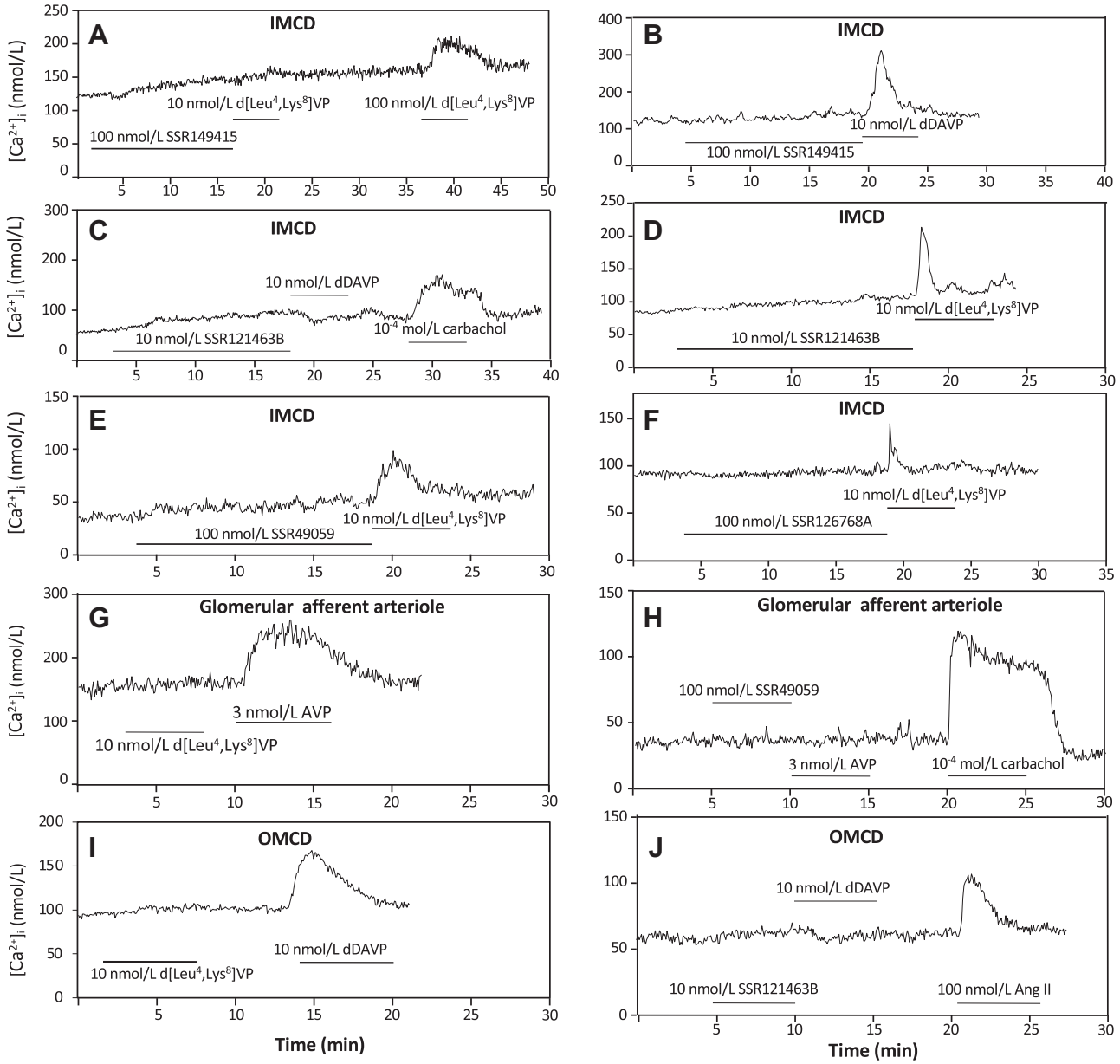

Figure 5. Pharmacology of the intracellular Ca^{2+} concentration ($[Ca^{2+}]_i$) responses induced by d[Leu^4, Lys^8]VP in various kidney structures. *A–F*: representative recordings of $[Ca^{2+}]_i$ levels in the inner medullary collecting duct (IMCD) elicited by 10 and 100 nmol/L d[Leu^4, Lys^8]VP after pretreatment with 100 nmol/L SSR149415 (*A*), 10 nmol/L 1-desamino-8-D-arginine vasopressin (dDAVP) after pretreatment with 100 nmol/L SSR149415 or 10 nmol/L SSR121463B (*B* and *C*), and 10 nmol/L d[Leu^4, Lys^8]VP after pretreatment with 10 nmol/L SSR121463B or 10 nmol/L d[Leu^4, Lys^8]VP or 100 nmol/L SSR49059 (*D–F*). *G* and *H*: representative recordings of $[Ca^{2+}]_i$ levels in glomerular afferent arterioles elicited by 10 nmol/L d[Leu^4, Lys^8]VP followed by 3 nmol/L arginine vasopressin (AVP) (*G*) and 3 nmol/L AVP after pretreatment with 100 nmol/L SSR49059 followed by 0.1 mol/L carbachol (*H*). *I* and *J*: representative recordings of $[Ca^{2+}]_i$ levels in the outer medullary collecting duct (OMCD) elicited by 10 nmol/L d[Leu^4, Lys^8]VP followed 10 nmol/L dDAVP (*I*) and 10 nmol/L dDAVP followed by 100 nmol/L angiotensin II after pretreatment with the V2 antagonist SSR121463B (*J*).

First, we tested the hypothesis of a cross talk between $hV_{1B}R$ and hV_2R. As shown in Fig. 8*A*, coexpression of increasing amounts of $hV_{1B}R$ cDNA with a constant amount of hV_2R cDNA synergized the V_2-cAMP response in a dose-dependent manner. Maximal potentiation (around 30%) was obtained for an $hV_{1B}R$-to-hV_2R ratio of 10. Interestingly, this potentiation was observed only on double-transfected cells and was completely blocked by preincubation with the V_{1B} antagonist SSR149415 (Fig. 8*B*). As a control, we verified on single hV_2R-transfected cells that SSR149415 did not modify the AVP-stimulated cAMP dose response (Fig. 8*C*). To further analyze which mechanism triggers hV_2R cAMP potentiation, we examined the effect of PMA, a potent PKC activator. PMA significantly potentiated AVP-stimulated cAMP accumulation in both hV_2R-transfected cells and $hV_{1B}R/hV_2R$ double-transfected cells (Fig. 8, *D* and *E*). Such an effect was blunted by the PKC inhibitor Gö6976 (Fig. 8*F*). All these data suggest that AVP, which stimulates PKC via $hV_{1B}R$ activation, may potentiated the AVP/cAMP response triggered by hV_2R stimulation.

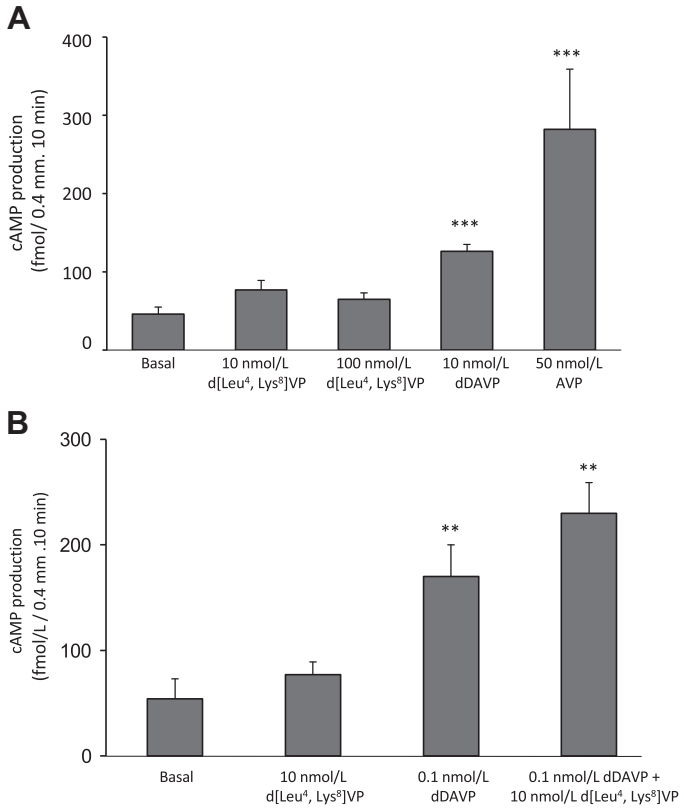

Figure 6. Effect of d[Leu^4, Lys^8]VP on intracellular cAMP accumulation in the inner medullary collecting duct. *A*: comparative effect of d[Leu^4, Lys^8]VP, 1-desamino-8-D-arginine vasopressin (dDAVP), and arginine vasopressin (AVP) on cAMP accumulation. Inner medullary collecting ducts were incubated with each vasopressin agonist. $n = 5–13$ independent determinations. *B*: additive effect of inframaximal doses of d[Leu^4, Lys^8]VP (10 nmol/L) and dDAVP (0.1 nmol/L) on cAMP accumulation. $n = 5–6$ independent determinations. Each bar represents the means ± SE of at least five determinations. ***$P < 0.001$ and **$P < 0.002$ vs. the basal value.

We have previously shown that $hV_{1B}R$ and hCRF1 receptor act in synergism involving cross talk at the level of second messengers and also receptor heterodimerization (26). In the present study, we verified whether $hV_2R/hV_{1B}R$ heterodimerization may also participate in the V_2/V_{1B} second messenger cross talk. Indeed, receptor-tagged versions $hV_{1B}RL$ and hV_2-EYFP expressed in HEK-293 cells led to similar cAMP results as nontagged vasopressin receptors (data not shown). HEK-293 cells were then cotransfected with $hV_{1B}RL$ and hV_2-YFP receptors, and physical interactions were challenged by direct BRET. As previously described (26), in the presence of $hV_{1B}RL$ as a donor, increasing concentrations of hCRF1-YFP as an acceptor led to a saturable curve indicating energy transfer (Fig. 9*A*). Transfection of hV_2-EYFP in the presence of $hV_{1B}RL$ showed a linear, nonsaturable curve of BRET, typical of that observed when no dimerization occurs, as was also observed for $hV_{1B}RL/hGABA_{B2}$-EYFP (Fig. 9*A*). The lack of $hV_{1B}R/hV_2R$ heterodimerization was confirmed by BRET competition experiments (Fig. 9*B*), as adding increasing amounts of DNA encoding untagged wild-type $hV_{1B}R$ to preexisting hV_2RL/hV_2-EYFP association was ineffective to interrupt the BRET signal, in contrast to $hV_{1A}R$ or hOTR known to heterodimerize with hV_2R (27). Such results indicate that the potentiation of the cAMP response induced by AVP in hV_2/hV_{1B}-cotransfected HEK-293 cells could not account for $V_2R/V_{1B}R$ heterodimerization.

Effect of Selective V_{1B} Agonist and Antagonist on Urinary Flow Rate

As shown in Table 1, acute administration of the V_{1B} agonist d[Leu^4, Lys^8]VP at a low dose (0.42 μg/kg) did not induced significant changes in urine flow rate and urine osmolality. In contrast, a higher dose (72 μg/kg) induced a marked increase in urine flow rate and decrease in urine osmolality in the V_{1B} agonist-treated group compared with the control group. The V_{1B} antagonist SSR149415 (30 mg/kg) did not significantly modify diuresis either in rats under basal conditions (2.9 ± 0.3 vs. 3.1 ± 0.4 mL/6 h in vehicle- and V_{1B} antagonist-treated groups, respectively) or in rats with high urine concentrating activity (pretreated for 5 days with Alzet minipumps delivering 400 ng/day AVP, 0.40 ± 0.14 vs. 0.30 ± 0.10 mL/6 h in vehicle- and V_{1B} antagonist-treated groups, respectively).

In Vivo Effect of VP Agonists on Rat Kidney Cell Proliferation

Higher cell proliferation assayed by BrdU incorporation was detected in medullary zones than in the cortex in control

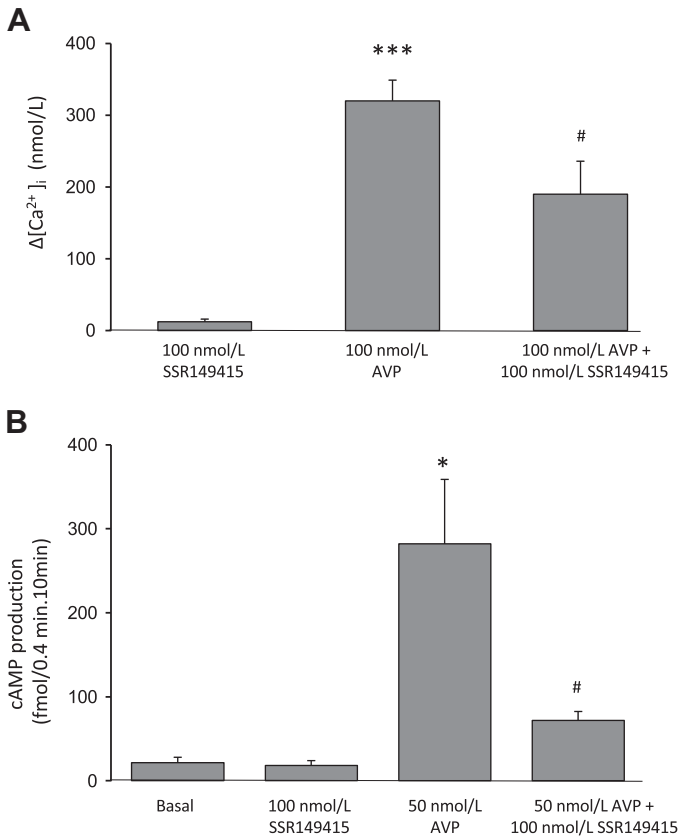

Figure 7. Effect of SSR149415 on intracellular Ca^{2+} mobilization and cAMP production induced by arginine vasopressin (AVP) in the inner medullary collecting duct. *A* and *B*: effect of the V_{1B} antagonist SSR149415 alone, AVP alone, or in combination on intracellular Ca^{2+} concentration ($[Ca^{2+}]_i$) (*A*) or cAMP production in the inner medullary collecting duct (*B*). Each bar represents the means ± SE of at least five independent determinations. *$P < 0.05$ and ***$P < 0.01$ vs. basal or SSR149415; #$P < 0.05$ vs. AVP.

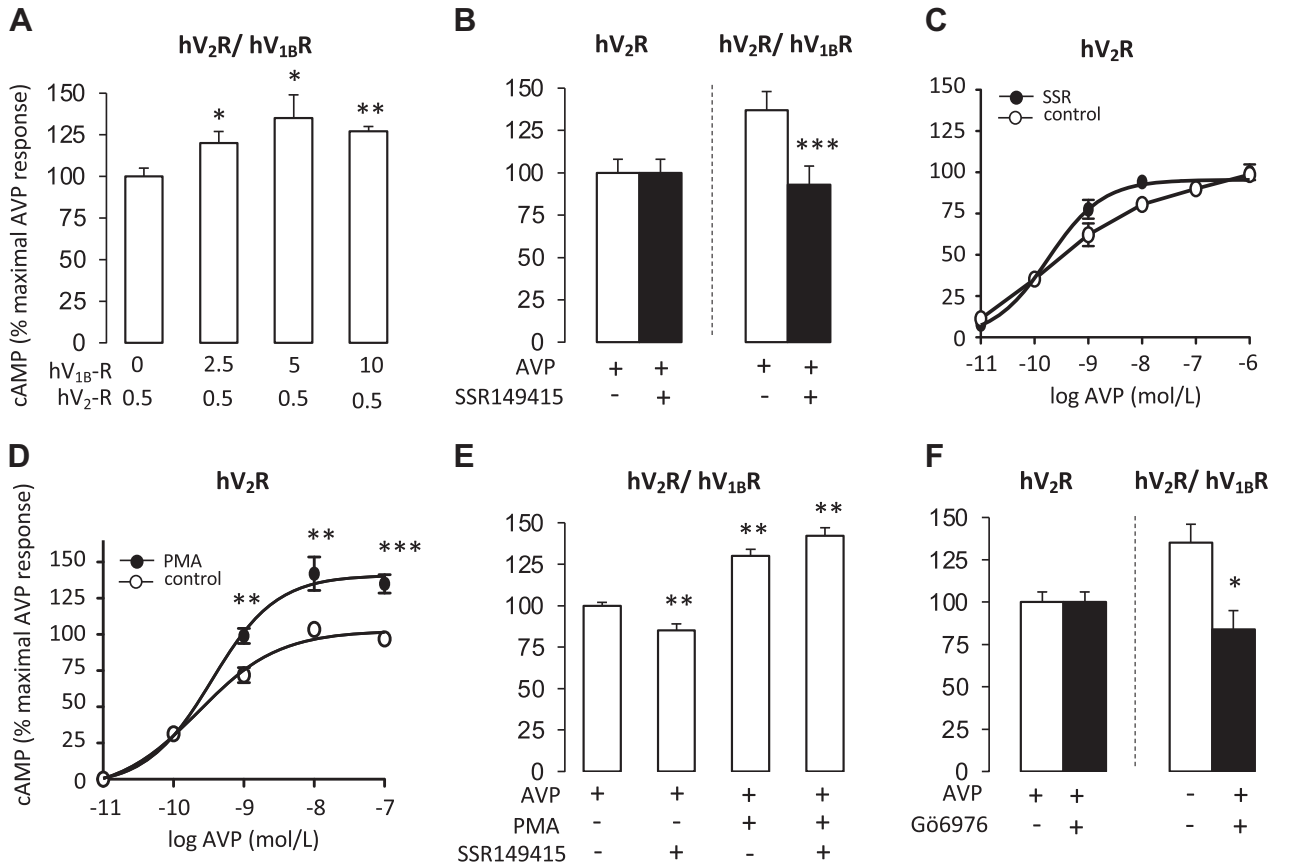

Figure 8. Second messenger synergism between human vasopressin V_2 and V_{1B} receptors (hV_2R and $hV_{1B}R$, respectively) in human embryonic kidney (HEK)-293 cells. Functional synergism between $hV_{1B}R$ and hV_2R was challenged by measuring cAMP accumulation induced by arginine vasopressin (AVP). HEK-293 cells were double transfected with 0.5 ng hV_2R and increasing amounts of $hV_{1B}R$ (0–10 ng; *A*) or with 1 ng hV_2R alone or cotransfected with 5 ng $hV_{1B}R$ (*B*–*F*). Accumulated cAMP was determined in the presence of 10 nmol/L AVP (*A*, *B*, *E*, and *F*) or increasing amounts of AVP (*C* and *D*) for a 30-min incubation period at 37°C. In *B* and *C*, a 15-min preincubation with or without 100 nmol/L SSR149415 (control) was performed before the AVP addition. In *D* and *E*, a 15-min preincubation without (control) or with 1 μmol/L PMA was performed before the AVP addition. In *F*, a 15-min preincubation period without (control) or with Gö6976 was performed before the AVP addition. In each condition, cAMP was measured and expressed as a percentage of the maximal AVP response over basal obtained for hV_2R single-transfected cells. Values are means ± SE of at least three distinct experiments each performed in triplicate. *$P < 0.05$, **$P < 0.01$, and ***$P < 0.001$ vs. control.

rats, and subcutaneous treatment with 2 μg/kg·day dDAVP strongly increased proliferation (near 4-fold) in each renal zone, as previously described (18). In contrast, treatment with 40 μg/kg·day d[Leu^4, Lys^8]VP did not significantly affected the rate of cell proliferation in each renal zone compared with saline treatment (Table 2).

DISCUSSION

Originality and New Data

The presence of the gene encoding $V_{1B}R$ within the renal medulla has been previously mentioned (14, 32, 33). For the first time, we identified and characterized $V_{1B}R$ in the IMCD using original ligands such as selective V_{1B} fluorescent or radioactive agonists and antagonist. Equilibrium binding experiments revealed a single high-affinity $V_{1B}R$ binding site that was present at low density. Functional experiments showed that agonist-induced stimulation of $V_{1B}R$ activates only the inositol 1,4,5-trisphosphate/Ca^{2+} signaling pathway and not cAMP production in the native IMCD. Furthermore, our results demonstrate a cross talk between $V_{1B}R$ and V_2R signaling pathways upon AVP stimulation in the freshly dissected rat IMCD.

Localization and Pharmacological Characterization of Kidney $V_{1B}R$

$V_{1B}R$ mRNA has been previously detected roughly in the rat medulla (14), but the specific cells expressing $V_{1B}R$ in this renal zone had not been investigated so far. Moreover, the absence of specific antibodies or labeled agonist hampered determination of the precise receptor $V_{1B}R$ protein localization along the nephron. Autoradiographic experiments with tritiated SSR149415 failed to detect $V_{1B}R$ in the human kidney, probably because of the weak specific activity of the tritiated ligand and of the low expression of $V_{1B}R$ in this organ (34). Using RT-PCR performed on microdissected nephron segments and using the fluorescent selective V_{1B} peptide d[Leu^4, Lys(Alexa647)^8]VP, we have shown that V_{1B} mRNA and protein are predominantly expressed in the IMCD and colocalized with AQP2 and V_2R.

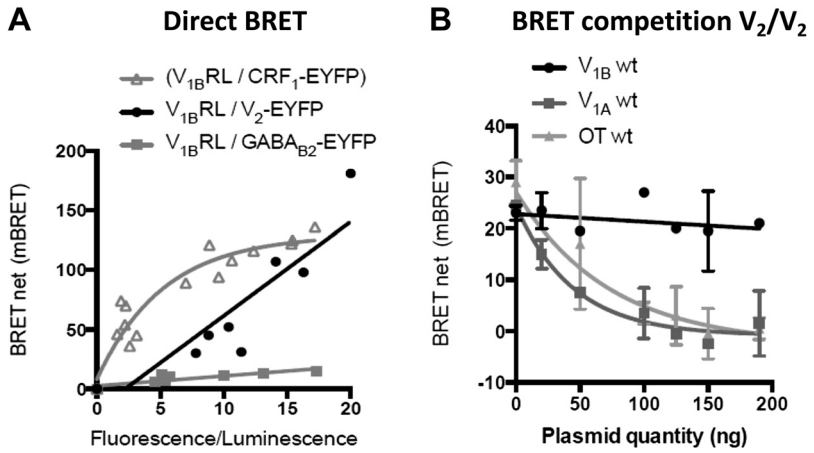

Figure 9. Challenging vasopressin V_{1B} receptor (V_{1B}R)/V_2 receptor (V_2R) heterodimerization. The human (h)V_{1B}R/hV_2R interaction was challenged by bioluminescence resonance energy transfer (BRET) saturation (*A*) or BRET competition (*B*) experiments. Human embryonic kidney-293 cells were cotransfected with plasmids encoding tagged or wild-type (wt) receptors and BRET was measured. For a direct interaction (BRET saturation), the donor hV_{1B}RLuc was incubated in the presence of increasing concentrations of an acceptor, namely, human corticotropin-releasing factor 1 (hCRF1)-enhanced yellow fluorescent protein (EYFP), hV_2-EYFP, or h$GABA_{B2}$-EYFP, and "BRET net" was measured in each condition. For BRET competition, a constant amount of hV_2RLuc/hV_2-EYFP known to give a positive BRET signal of homodimerization (27) was incubated with increasing concentrations of plasmids encoding different unlabeled acceptors, i.e., wild-type hV_{1B}R, hV_1R, or human oxycotin receptor (hOTR). The potential decreases of "BRET net" as a function of the dose of the unlabeled acceptor were then measured. Values are means ± SE of at least three independent experiments, each performed in triplicate.

The use of the tritiated form of d[Leu^4, Lys^8]VP corroborated the presence of V_{1B}R within the IM. The pharmacological properties of the selective binding sites detected in the IM fit well with those of V_{1B}R, exhibiting a subnanomolar affinity for d[Leu^4, Lys^8]VP and an affinity in the nanomolar range for the selective V_{1B}R antagonist SSR149415 (31). However, V_{1B}R expression is very low (19 fmol/mg protein) compared with V_2R in the rat IM (493 fmol/mg protein) (35) or with V_{1B}R in the rat pituitary (150–300 fmol/mg protein) (32).

Ca^{2+} and cAMP Signaling Pathways Associated With V_{1B}R in the IMCD

To better preserve the coupling properties of the receptor and to analyze the mechanisms that really occurred in vivo, our experiments were performed on the freshly microdissected IMCD, preserving the structural integrity of the CD. Moreover, to be sure that we selectively activated V_{1B}R, which is coexpressed at low density with V_2R in this structure, we carefully verified the pharmacological specificity of the analogs, as we previously have shown that dDAVP is considered as a mixed V_2/V_{1B} agonist depending on the dose used (31). Our signaling experiments showed that stimulation of V_{1B}R by d[Leu^4, Lys^8]VP is directly coupled to an increase in intracellular Ca^{2+} mobilization. This effect is dose dependent and saturable with a nanomolar affinity constant. In the absence of extracellular Ca^{2+}, the persistence of a spike of the $[Ca^{2+}]_i$ response to d[Leu^4, Lys^8]VP indicated that the initial increase in $[Ca^{2+}]_i$ originated from the mobilization of intracellular pools. The role of extracellular Ca^{2+} entry was evidenced in Ca^{2+}-free medium by a significant reduction of the peak response and the steady-state sustained increase in $[Ca^{2+}]_i$. Thus, V_{1B}R-induced elevation of $[Ca^{2+}]_i$ in the IMCD is dependent on both intracellular and extracellular Ca^{2+} pools, similarly to V_{1A}R in primary cultures of rat adrenal glomerulosa cells both coupled to the phospholipase C pathway and to voltage-activated Ca^{2+} channels (36).

In contrast, we observed that V_{1B}R activation by d[Leu^4, Lys^8]VP even at a high concentration did not increase cAMP production. Such results are in agreement with an earlier

Table 1. *Effect of the vasopressin V_{1B} receptor agonist d[Leu^4, Lys^8]VP on urine volume, urine osmolality, and urinary osmolar excretion during the 5 h after compound administration*

	Volume, mL	Osmolality, mOsm/kgH_2O	Osmolar Excretion, μOsm
Vehicle	1.9 ± 0.3	2,235 ± 93	4,094 ± 602
d[Leu^4, Lys^8]VP, (0.42 μg/kg)	2.7 ± 0.6	1,705 ± 272	4,133 ± 385
Vehicle	1.2 ± 0.2	2,150 ± 88	2,448 ± 241
d[Leu^4, Lys^8]VP (72 μg/kg)	6.9 ± 0.7†	534 ± 10†	3,596 ± 124*

Results are means ± SE; n = 5/group. *$P < 0.05$ and †$P < 0.001$ vs. the corresponding vehicle-treated group.

Table 2. *Effect of 3 days of treatment with vasopressin V_{1B} receptor agonist d[Leu^4, Lys^8]VP or the V_2 receptor agonist dDAVP on renal cell proliferation*

	Control	d[Leu^4, Lys^8]VP (40 μg/kg·day)	dDAVP (2 μg/kg·day)
Cortex	15 ± 4	26 ± 8	79 ± 8*
Outer medulla	37 ± 3	60 ± 15	210 ± 15*
Inner medulla	68 ± 7	90 ± 8	307 ± 23†

Results are means ± SE of the number of bromodeoxyuridine-labeled nuclei counted within a 500-μm side-squared field centered on the different kidney regions on 4 sections/animal and 4 animals/group. dDAVP, 1-desamino-8-D-arginine vasopressin. *$P < 0.05$ and †$P < 0.001$ vs. the respective zone in the control group.

study showing that $V_{1B}R$ present in the rat pituitary is not coupled to adenylate cyclase (AC) (37). A discrete activation of both cAMP and Ca^{2+} pathways was only detected in transfected cell lines stably expressing a very high level of $V_{1B}R$ (38) compared with native tissues analyzed in the present study. If $V_{1B}R$ stimulation does not stimulate cAMP accumulation per se when using a selective V_{1B} agonist (Fig. 6), it plays an important role in modulating the AVP-stimulated cAMP response. This is clearly evidenced in Fig. 7, which shows that SSR149415 strongly inhibited AVP-stimulated cAMP production. This implies that the AVP-stimulated cAMP response is due to both V_2R and $V1_BR$ activation.

Cross Talk Between $V_{1B}R$ and V_2R Signaling Pathways

It is clear that a balance between intracellular cAMP and Ca^{2+} concentrations represents the key factor for regulating water permeability of the principal cells of the renal tubule (9, 10). Molecular studies earlier performed on this structure or presented in this article allow a better understanding of how the intricacy between the two second messenger pathways associated with V_2R and $V_{1B}R$ stimulation may account for the complex physiological actions of AVP on the IMCD.

As $V_{1B}R$ and V_2R are coexpressed in the same IMCD cells and as AVP has the same affinity for both receptors (31), it is tempting to speculate that, in this segment, both $V_{1B}R$ and V_2R are involved in the physiological action of AVP. Indeed, we showed that each receptor stimulated by its selective agonist increases $[Ca^{2+}]_i$ and that these respective responses are independent, as additive when inframaximal doses of dDAVP or d[Leu^4, Lys^8]VP were used. Such results are in agreement with the partial inhibitory effect of SSR149415 on the AVP-stimulated $[Ca^{2+}]_i$ increase acting only on the V_{1B}-sensitive part of the global Ca^{2+} response. In contrast, the cooperation between the two receptor isoforms concerns the cAMP pathways as although the V_{1B} agonist d[Leu^4, Lys^8]VP cannot trigger per se cAMP production, the selective V_{1B} antagonist SSR149415 strongly reduced AVP-stimulated cAMP production (Fig. 7).

Two hypotheses may be proposed to explain these observations. The first hypothesis is the heterodimerization of V_2R and $V_{1B}R$ leading to a receptor complex exhibiting novel coupling properties. Thus, $V_{1A}R$, V_2R, and OTR have been previously shown to constitute both homo- and heterodimers (27). In HEK-293 cells cotransfected with $hV_{1B}R$ and hCRF1 receptor, which exhibit the same type of coupling than those of $V_{1B}R$ and V_2R (Gq and Gs, respectively), receptor heterodimerization induced a synergistic noncanonical coupling (26). However, direct BRET and competition BRET assays performed in the present study did not support a dimerization $V_{1B}R$ and V_2R. Obviously, such experiments were performed on human but not rat vasopressin receptors. Yet, as previously discussed in this study, human and rat $V_{1B}R$ and V_2R exhibit very strong structural and functional similarities. Moreover, as shown in this study, the V_{1B} potentiating effect on AVP-stimulated cAMP accumulation was observed both on the freshly dissected rat IMCD and HEK-289 cells double transfected with hV_2R and $hV_{1B}R$ (Figs. 7 and 8).

The second hypothesis would be a cross talk between second messenger cascades triggered by concomitant V_2R and $V_{1B}R$ activation. Many arguments favored such explanation. Thus, the comparison of maximal cAMP accumulation obtained on crude plasma membranes derived from the IM with those obtained on the freshly dissected IMCD is very interesting. On crude plasma membranes from the rat IM, the specific V_2 agonist dDAVP induced maximal cAMP production quite similar (88%) to that obtained with AVP (30). In contrast, on intact principal cells from the freshly microdissected IMCD, this ratio was only of 53% (this study). This discrepancy probably arises from the ability of AVP to induce increases in both $[Ca^{2+}]_i$ and DAG production in the microdissected IMCD where the cellular integrity is maintained, whereas in the membrane assay, the Ca^{2+}- and DAG-potentiating effect is suppressed.

A nonexhaustive review of the literature also supports such a cross talk hypothesis as in the rat IMCD, the importance of Ca^{2+} influx and/or intracellular Ca^{2+} mobilization from internal stores on AC or PDE activities able to regulate intracellular cAMP content is well documented. In this tissue, cAMP generation is controlled by different AC exhibiting opposite sensitivity to Ca^{2+}. It is now well established that the AC6 isoform is expressed all along the CD together with AC5 only present in the OMCD and CCD. Both isoforms are functionally active since an increase of Ca^{2+} influx inhibited cAMP accumulation (39). More recently, functional Ca^{2+}/calmodulin-sensitive AC3 blocked by specific calmodulin inhibitors has also been discovered (40). Distinct PDEs responsible for the hydrolysis of cAMP are also expressed in the renal CD and play an important role. If PDE1, PDE3, and PDE4 are present in the renal CD (41), PDE4 is more particularly involved in regulating AVP-stimulated cAMP degradation (42). Yet, as PDE1 is activated by a Ca^{2+}/calmodulin process (43), the increase of intracellular Ca^{2+} induced by both V_2R and $V_{1B}R$ activation in the IMCD (see Fig. 3) may also participate in a feedback of cAMP production triggered by V_2R activation. Similarly, PKA activated by cAMP was shown to stimulate PDE4 activity, leading thus to another negative feedback of the cAMP pathway (44). The intracellular Ca^{2+} increase due to $V_{1B}R$ activation may also have a negative feedback on cAMP accumulation driven by V_2R activation indirectly via a stimulation of prostaglandin E_2 synthesis known to inhibit cAMP production via a complex mechanism involving an increase of PDE expression (45).

The role of PKC activation induced upon $V_{1B}R$ activation may also explain the cross talk between V_2R and $V_{1B}R$. Indeed, a study performed by Ishikawa et al. (46) on rat renal papillary collecting tubule cells in culture showed that PMA, a PKC activator like DAG, can modulate basal cAMP production. We tried to reproduce these experiments in our freshly microdissected IMCD, but clearly this tissue does not represent an appropriate model for studying cross-talk mechanisms due to the limited amounts of tissues available and the relative higher dispersion of cAMP data compared with those obtained on cell culture. We thus performed such experiments on $hV_{1B}R/hV_2R$ double-transfected HEK-293 cells. We showed on this heterologous cellular model that PMA potentiates hV_2 cAMP accumulation induced by AVP. Moreover, the use of Gö6958, a PKC inhibitor, blunted the cAMP potentiating effect of $hV_{1B}R$ activation by the hV_2 response (Fig. 8*F*). Taken together, these data strongly suggest the role of PKC in the fine tune regulation of hV_2R-induced cAMP accumulation.

Our data obtained from both a heterologous cellular model and freshly dissected IMCD tubules clearly show that both positive and negative regulation loops contribute to the global response to AVP stimulation. However, it is difficult to precisely define the level of intricacy between the Ca^{2+} and cAMP pathways inside principal cells of the IMCD as *1*) our cAMP measurements concerned cell lysates and the Ca^{2+} signal was obtained on whole IMCD fragments and *2*) the two second messenger responses exhibit different spatial and temporal patterns in living cells due namely to different subcellular distributions of the enzymes involved in second messenger generation like AC, PDE, protein kinases, and Ca^{2+} channels. Only a spatial- and temporal-controlled second messenger production performed on IMCD principal cells would allow a better comprehension of precise mechanisms by which vasopressin second messenger cascades at the cellular level.

Physiological and Pathophysiological Roles of $V_{1B}R$ in the Kidney

Together with previous studies performed on freshly dissected CDs or primary cultures from the IMCD from the rat male kidney, our data allow a better understanding of the complex mechanisms by which vasopressin regulates water reabsorption by interacting with both well-characterized renal V_2R and also with other vasopressin/OT receptors also expressed in this organ, like the V_{1B} isoform extensively characterized in this study.

Vasopressin at very low doses (0.1 nmol/L) strongly stimulates cAMP production (47). At this concentration, a small $[Ca^{2+}]_i$ response has been described. This dual effect is clearly mediated by V_2R as it is mimicked by the selective V_2 agonist dDAVP and blocked by selective V_2 antagonist (Fig. 5*J*) (47, 48). In this context, the respective role of cAMP and $[Ca^{2+}]_i$ increase in regulating renal water permeability may be better understood. First, the interaction of AVP with V_2R stimulates AC activity via a Gs stimulatory process (7) and leads to cAMP accumulation. Such an increase stimulates the activity of PKA, which then phosphorylates AQP2, a step necessary to induce its translocation to the apical membrane of principal collecting tubule cell and responsible for increasing osmotic water permeability. If cAMP represents the main intracellular messenger triggering the hormonal effect, it has been elegantly demonstrated that the small increase of $[Ca^{2+}]_i$ is also important as IMCD preincubation with an intracellular Ca^{2+} chelator inhibits the AVP-stimulated $[Ca^{2+}]_i$ increase and osmotic water permeability. Moreover, this $[Ca^{2+}]_i$ increases acts downstream of AC stimulation, as the intracellular Ca^{2+} chelator did not inhibit AVP-stimulated cAMP production and permeant cAMP analogs have been described to mimic the small $[Ca^{2+}]_i$ increase (48). Such a Ca^{2+} increase originates from ryanodine-sensitive intracellular stores activated by cAMP and not from intracellular inositol 1,4,5-trisphosphate-sensitive stores (49). The authors showed that this Ca^{2+} increase favored AQP2 translocation to the apical membrane via a calmodulin kinase-dependent process facilitating osmotic water permeability (48).

For higher AVP concentrations (10 nmol/L and above), AVP still stimulates cAMP production to the same level as that obtained with 0.1 nmol/L (Fig. 3) (47). Using such high AVP concentrations, we and others (9–11) have observed the development of a robust and reproducible Ca^{2+} signal. No saturation of the AVP Ca^{2+} response was observed even at 10 or 100 nmol/L (Fig. 3) (11), suggesting an EC_{50} value higher than 20 nmol/L. On the freshly microdissected rat IMCD, it was also shown that at supraananomolar concentration, hormones mobilizing Ca^{2+} would inhibit osmotic water permeability (12). The authors suggested that such an important Ca^{2+} increase may counterbalance the osmotic effect induced by low vasopressin concentration that mainly stimulates cAMP production via V_2R activation. Such a hypothesis may explain *1*) the bell-shaped dose-response curve obtained in vivo by measuring antidiuresis upon AVP injection in the rat (50) and *2*) the classical antidiuretic saturation dose-response curve obtained with dDAVP known to strongly stimulate cAMP production and more weakly maximal $[Ca^{2+}]_i$ increase compared with AVP (this study and Ref. 50). In the light of these results, we propose that high vasopressin concentrations able to induce a Ca^{2+} response via $V_{1B}R$ activation may counterbalance the well-known antidiuretic effects induced by AVP interaction with V_2R. Nevertheless, this effect is probably weak according to the low density of $V_{1B}R$ that we measured compared with that of V_2R.

Such an interpretation may also explain the intriguing effects that we observed in vivo on diuresis with V_{1B} agonist. In normohydrated rats with a relatively low concentration of AVP, the changes in $[Ca^{2+}]_i$ induced by low doses of the $V_{1B}R$ agonist d(Leu^4, Lys^8)VP (0.42 µg/kg) were too weak to notably alter the antidiuretic V_2R effect. Accordingly, previous studies have shown in rats under normal conditions that acute administration of 0.05 nmol/100g d(Leu^4, Lys^8)VP, a similar dosage as we used, did not modify urinary flow rate or electrolyte excretion (51, 52). At high doses (72 µg/kg), d(Leu^4, Lys^8)VP probably induced a maximal Ca^{2+} response known to modulate osmotic water permeability and thus a significant effect on diuresis (Table 1). However, a central effect of a high dose of d(Leu^4, Lys^8)VP could not be excluded in this condition, as activation of pituitary $V_{1B}R$ leads to an increase in CRF and adenocorticotropic hormone production (53), consequently an increase in corticosteroid secretion (54), and secondarily an increase in water intake and diuresis (55).

Analogously to the absence of diuretic effect of low doses of d(Leu^4, Lys^8)VP, SSR149415 did not change urine flow rate in normal rats. Indeed, under basal conditions, the circulating level of AVP is too low to stimulate $V_{1B}R$. Consequently, SSR149415 could not to prevent AVP binding on $V_{1B}R$ and is inefficient on diuresis. As expected, SSR149415 treatment also did not change urine flow rate in homozygous Brattleboro rats devoid of AVP (C. Serradeil-Le Gal, personal communication). Noticeably, the antidiuretic effect of SR49059, a selective $V_{1A}R$ antagonist that prevents AVP-stimulated intracellular Ca^{2+} mobilization, has been highlighted only in rats with a high plasma AVP concentration (50).

A noteworthy previous study has reported a daily higher urine volume in mice lacking $V_{1B}R$ compared with control mice (19). The apparent discrepancy with our results on the acute diuretic effects of $V_{1B}R$ stimulation may be explained either by species differences in $V_{1B}R$ density and/or in renal pattern or, more probably, by the complex interactions between receptor signaling and compensatory mechanisms

that occur in the lifelong absence of one component of the vasopressin system.

Overall, our results indicate that under physiological conditions, the plasmatic concentration of AVP mainly stimulates V_2R activation, thus producing cAMP mainly responsible for osmotic water permeability. For higher plasmatic concentrations, AVP may both activate V_2R, $V_{1A}R$ expressed in the OMCD (56), and V_2R, $V_{1B}R$, and OTR coexpressed in the IMCD (this study and Ref. 57), as AVP is an agonist of nanomolar affinity for all these vasopressin/OT receptor isoforms (31). This concerted activation of kidney vasopressin/OT receptors tightly coupled to $[Ca^{2+}]_i$ may counterbalance the antidiuretic effect of AVP triggered by V_2R activation. Obviously, the densities of each of these receptors are low compared with those of V_2R, but, by acting all together in different kidney regions where V_2R is expressed, they may produce a fine-tuned regulation of vasopressin antidiuretic activity in some pathophysiological conditions in which the plasmatic AVP concentration is largely increased, like in syndrome of inappropriate antidiuretic hormone secretion or severe dehydration.

In conclusion, this study clearly demonstrated the presence of low amounts of functional $V_{1B}R$ in the IMCD coexpressed with V_2R and AQP2 in the same principal cells. These data contribute to our understanding of how $V_{1B}R$ may cooperate with V_2R to finely regulate cAMP and Ca^{2+} signaling pathways in a native biological model.

ACKNOWLEDGMENTS

We thank Dr. M. Manning for providing the vasopressin peptidic agonists, Dr. D. Devost and Dr. M. Bouvier for providing the vasopressin receptor probes, Sanofi Toulouse for the generous gift of nonpeptide vasopressin antagonists, and Lise Bankir for fruitful discussions.

GRANTS

This work was supported by Institut National de la Santé et de la Recherche Médicale, Centre National de la Recherche Scientifique, Collège de France, Université de Montpellier, Université de Paris ANR-18-IDEX-0001, and National Research Development and Innovation Office K124952.

DISCLOSURES

No conflicts of interest, financial or otherwise, are declared by the authors.

AUTHOR CONTRIBUTIONS

A.H-C., N.B., C.L-C., and G.G. conceived and designed research; A.H-C., N.B., M.C., J.M., C.M., J.D., C.T., and M.T. performed experiments; A.H-C., N.B., J.M., C.S-L.G., C.L-C., and G.G. analyzed data; A.H-C., N.B., M.T., C.L-C., and G.G. interpreted results of experiments; A.H-C., N.B., M.C., C.M., G.G. prepared figures; A.H-C., N.B., and G.G. drafted manuscript; A.H-C., N.B., C.T., M.T., C.L-C., and G.G., edited and revised manuscript; A.H-C., N.B., M.C., J.M., C.M., J.D., C.T., M.T., C.S-L.G., C.L-C., and G.G., approved final version of manuscript.

REFERENCES

1. **Bankir L.** Antidiuretic action of vasopressin: quantitative aspects and interaction between V1a and V2 receptor-mediated effects. *Cardiovasc Res* 51: 372–390, 2001. doi:10.1016/s0008-6363(01)00328-5.
2. **Holmes CL**, **Landry DW**, **Granton JT.** Science review: vasopressin and the cardiovascular system part 1–receptor physiology. *Crit Care* 7: 427–434, 2003. doi:10.1186/cc2337.
3. **Young LJ**, **Wang Z.** The neurobiology of pair bonding. *Nat Neurosci* 7: 1048–1054, 2004. doi:10.1038/nn1327.
4. **Koshimizu TA**, **Tsujimoto G.** New topics in vasopressin receptors and approach to novel drugs: vasopressin and pain perception. *J Pharmacol Sci* 109: 33–37, 2009. doi:10.1254/jphs.08r18fm.
5. **Thibonnier M**, **Preston JA**, **Dulin N**, **Wilkins PL**, **Berti-Mattera LN**, **Mattera R.** The human V3 pituitary vasopressin receptor: ligand binding profile and density-dependent signaling pathways. *Endocrinology* 138: 4109–4122, 1997. doi:10.1210/endo.138.10.5432.
6. **Jard S.** Vasopressin receptors. A historical survey. In: *Vasopressin and Oxytocin. Advances in Experimental Medicine and Biology*, edited by Zingg HH, Bourque CW, Bichet DG**.** Boston, MA: Springer, 1998, vol 449, p. 1–13. https://doi.org/10.1007/978-1-4615-4871-3_1.
7. **Guillon G**, **Butlen D**, **Cantau B**, **Barth T**, **Jard S.** Kinetic and pharmacological characterization of vasopressin membrane receptors from human kidney medulla: relation to adenylate cyclase activation. *Eur J Pharmacol* 85: 291–304, 1982. doi:10.1016/0014-2999(82)90216-3.
8. **Birnbaumer M**, **Seibold A**, **Gilbert S**, **Ishido M**, **Barberis C**, **Antaramian A**, **Brabet P**, **Rosenthal W.** Molecular cloning of the receptor for human antidiuretic hormone. *Nature* 357: 333–335, 1992. doi:10.1038/357333a0.
9. **Star RA**, **Nonoguchi H**, **Balaban R**, **Knepper MA.** Calcium and cyclic adenosine monophosphate as second messengers for vasopressin in the rat inner medullary collecting duct. *J Clin Invest* 81: 1879–1888, 1988. doi:10.1172/JCI113534.
10. **Ishikawa S**, **Okada K**, **Saito T.** Arginine vasopressin increases cellular free calcium concentration and adenosine 3',5'-monophosphate production in rat renal papillary collecting tubule cells in culture. *Endocrinology* 123: 1376–1384, 1988. doi:10.1210/endo-123-3-1376.
11. **Maeda Y**, **Han JS**, **Gibson CC**, **Knepper MA.** Vasopressin and oxytocin receptors coupled to Ca^{2+} mobilization in rat inner medullary collecting duct. *Am J Physiol Renal Physiol* 265: F15–F25, 1993. doi:10.1152/ajprenal.1993.265.1.F15.
12. **Han JS**, **Maeda Y**, **Knepper MA.** Dual actions of vasopressin and oxytocin in regulation of water permeability in terminal collecting duct. *Am J Physiol Renal Physiol* 265: F26–F34, 1993. doi:10.1152/ajprenal.1993.265.1.F26.
13. **Champigneulle A**, **Siga E**, **Vassent G**, **Imbert-Teboul M.** V2-like vasopressin receptor mobilizes intracellular Ca^{2+} in rat medullary collecting tubules. *Am J Physiol Renal Physiol* 265: F35–F45, 1993. doi:10.1152/ajprenal.1993.265.1.F35.
14. **Saito M**, **Tahara A**, **Sugimoto T**, **Abe K**, **Furuichi K.** Evidence that atypical vasopressin V(2) receptor in inner medulla of kidney is V(1B) receptor. *Eur J Pharmacol* 401: 289–296, 2000. doi:10.1016/s0014-2999(00)00465-9.
16. **Yang B**, **Bankir L.** Urea and urine concentrating ability: new insights from studies in mice. *Am J Physiol Renal Physiol* 288: F881–F896, 2005. doi:10.1152/ajprenal.00367.2004.
17. **Fenton RA.** Essential role of vasopressin-regulated urea transport processes in the mammalian kidney. *Pflugers Arch* 458: 169–177, 2009. doi:10.1007/s00424-008-0612-4.
18. **Alonso G**, **Galibert E**, **Boulay V**, **Guillou A**, **Jean A**, **Compan V**, **Guillon G.** Sustained elevated levels of circulating vasopressin selectively stimulate the proliferation of kidney tubular cells via the activation of V2 receptors. *Endocrinology* 150: 239–250, 2009. doi:10.1210/en.2008-0068.
19. **Daikoku R**, **Kunitake T**, **Kato K**, **Tanoue A**, **Tsujimoto G**, **Kannan H.** Body water balance and body temperature in vasopressin V1b receptor knockout mice. *Auton Neurosci* 136: 58–62, 2007. doi:10.1016/j.autneu.2007.04.002.
20. **Corbani M**, **Trueba M**, **Stoev S**, **Murat B**, **Mion J**, **Boulay V**, **Guillon G**, **Manning M.** Design, synthesis, and pharmacological characterization of fluorescent peptides for imaging human V1b vasopressin or oxytocin receptors. *J Med Chem* 54: 2864–2877, 2011. doi:10.1021/jm1016208.
21. **Chafai M**, **Corbani M**, **Guillon G**, **Desarménien MG.** Vasopressin inhibits LTP in the CA2 mouse hippocampal area. *PLoS One* 7: e49708, 2012. doi:10.1371/journal.pone.0049708.

22. **Corbani M**, **Marir R**, **Trueba M**, **Chafai M**, **Vincent A**, **Borie AM**, **Desarmenien MG**, **Ueta Y**, **Tomboly C**, **Olma A**, **Manning M**, **Guillon G.** Neuroanatomical distribution and function of the vasopressin V1B receptor in the rat brain deciphered using specific fluorescent ligands. *Gen Comp Endocrinol* 258: 15–32, 2018. doi:10.1016/j.ygcen.2017.10.011.
23. **Le Bouffant F**, **Hus-Citharel A**, **Morel F.** Metabolic CO_2 production by isolated single pieces of rat distal nephron segments. *Pflugers Arch* 401: 346–353, 1984. doi:10.1007/BF00584334.
24. **Helou CM**, **Marchetti J.** Morphological heterogeneity of renal glomerular arterioles and distinct $[Ca^{2+}]_i$ responses to ANG II. *Am J Physiol* 273: F84–F96, 1997. doi:10.1152/ajprenal.1997.273.1.F84.
25. **Hus-Citharel A**, **Bodineau L**, **Frugière A**, **Joubert F**, **Bouby N**, **Llorens-Cortes C.** Apelin counteracts vasopressin-induced water reabsorption via cross talk between apelin and vasopressin receptor signaling pathways in the rat collecting duct. *Endocrinology* 155: 4483–4493, 2014. doi:10.1210/en.2014-1257.
26. **Murat B**, **Devost D**, **Andrés M**, **Mion J**, **Boulay V**, **Corbani M**, **Zingg HH**, **Guillon G.** V1b and CRHR1 receptor heterodimerization mediates synergistic biological actions of vasopressin and CRH. *Mol Endocrinol* 26: 502–520, 2012. doi:10.1210/me.2011-1202.
27. **Terrillon S**, **Durroux T**, **Mouillac B**, **Breit A**, **Ayoub MA**, **Taulan M**, **Jockers R**, **Barberis C**, **Bouvier M.** Oxytocin and vasopressin V1a and V2 receptors form constitutive homo- and heterodimers during biosynthesis. *Mol Endocrinol* 17: 677–691, 2003. doi:10.1210/me.2002-0222.
28. **Nielsen S**, **DiGiovanni SR**, **Christensen EI**, **Knepper MA**, **Harris HW.** Cellular and subcellular immunolocalization of vasopressin-regulated water channel in rat kidney. *Proc Natl Acad Sci USA* 90: 11663–11667, 1993. doi:10.1073/pnas.90.24.11663.
29. **Vagnes OB**, **Hansen FH**, **Feng JJ**, **Iversen BM**, **Arendshorst WJ.** Enhanced Ca^{2+} response to AVP in preglomerular vessels from rats with genetic hypertension during different hydration states. *Am J Physiol Renal Physiol* 288: F1249–F1256, 2005. doi:10.1152/ajprenal.00363.2004.
30. **Butlen D**, **Guillon G**, **Rajerison RM**, **Jard S**, **Sawyer WH**, **Manning M.** Structural requirements for activation of vasopressin-sensitive adenylate cyclase, hormone binding, and antidiuretic actions: effects of highly potent analogues and competitive inhibitors. *Mol Pharmacol* 14: 1006–1017, 1978. doi:10.1016/0014-2999(84)90314-5.
31. **Manning M**, **Misicka A**, **Olma A**, **Bankowski K**, **Stoev S**, **Chini B**, **Durroux T**, **Mouillac B**, **Corbani M**, **Guillon G.** Oxytocin and vasopressin agonists and antagonists as research tools and potential therapeutics. *J Neuroendocrinol* 24: 609–628, 2012. doi:10.1111/j.1365-2826.2012.02303.x.
32. **Lolait SJ**, **Stewart LQ**, **Jessop DS**, **Young WS 3rd**, **O'Carroll AM.** The hypothalamic-pituitary-adrenal axis response to stress in mice lacking functional vasopressin V1b receptors. *Endocrinology* 148: 849–856, 2007. doi:10.1210/en.2006-1309.
33. **Kutina AV**, **Makashov AA**, **Balbotkina EV**, **Karavashkina TA**, **Natochin YV.** Subtypes of Neurohypophyseal Nonapeptide Receptors and Their Functions in Rat Kidneys. *Acta Naturae* 12: 73–83, 2020. doi:10.32607/actanaturae.10943.
34. **Serradeil-Le Gal C**, **Raufaste D**, **Derick S**, **Blankenstein J**, **Allen J**, **Pouzet B**, **Pascal M**, **Wagnon J**, **Ventura MA.** Biological characterization of rodent and human vasopressin V1b receptors using SSR-149415, a nonpeptide V1b receptor ligand. *Am J Physiol Regul Integr Comp Physiol* 293: R938–R949, 2007. doi:10.1152/ajpregu.00062.2007.
35. **Ali M**, **Guillon G**, **Cantau B**, **Balestre MN**, **Chicot D**, **Clos J.** A comparative study of plasma vasopressin levels and V1 and V2 vasopressin receptor properties in congenital hypothyroid rat under thyroxine or vasopressin therapy. *Horm Metab Res* 19: 624–628, 1987. doi:10.1055/s-2007-1011895.
36. **Grazzini E**, **Lodboerer AM**, **Perez-Martin A**, **Joubert D**, **Guillon G.** Molecular and functional characterization of V1b vasopressin receptor in rat adrenal medulla. *Endocrinology* 137: 3906–3914, 1996. doi:10.1210/endo.137.9.8756565.
37. **Guillon G**, **Gaillard RC**, **Kehrer P**, **Schoenenberg P**, **Muller AF**, **Jard S.** Vasopressin and angiotensin induce inositol lipid breakdown in rat adenohypophysial cells in primary culture. *Regul Pept* 18: 119–129, 1987. doi:10.1016/0167-0115(87)90001-2.
38. **Orcel H**, **Albizu L**, **Perkovska S**, **Durroux T**, **Mendre C**, **Ansanay H**, **Mouillac B**, **Rabie A.** Differential coupling of the vasopressin V1b receptor through compartmentalization within the plasma membrane. *Mol Pharmacol* 75: 637–647, 2009. doi:10.1124/mol.108.049031.
39. **Chabardès D**, **Firsov D**, **Aarab L**, **Clabecq A**, **Bellanger AC**, **Siaume-Perez S**, **Elalouf JM.** Localization of mRNAs encoding Ca^{2+}-inhibitable adenylyl cyclases along the renal tubule. Functional consequences for regulation of the cAMP content. *J Biol Chem* 271: 19264–19271, 1996. doi:10.1074/jbc.271.32.19264.
40. **Hoffert JD**, **Chou CL**, **Fenton RA**, **Knepper MA.** Calmodulin is required for vasopressin-stimulated increase in cyclic AMP production in inner medullary collecting duct. *J Biol Chem* 280: 13624–13630, 2005. doi:10.1074/jbc.M500040200.
41. **Wang X**, **Ward CJ**, **Harris PC**, **Torres VE.** Cyclic nucleotide signaling in polycystic kidney disease. *Kidney Int* 77: 129–140, 2010. doi:10.1038/ki.2009.438.
42. **Pinto CS**, **Raman A**, **Reif GA**, **Magenheimer BS**, **White C**, **Calvet JP**, **Wallace DP.** Phosphodiesterase isoform regulation of cell proliferation and fluid secretion in autosomal dominant polycystic kidney disease. *J Am Soc Nephrol* 27: 1124–1134, 2016. doi:10.1681/ASN.2015010047.
43. **Goraya TA**, **Cooper DM.** Ca^{2+}-calmodulin-dependent phosphodiesterase (PDE1): current perspectives. *Cell Signal* 17: 789–797, 2005. doi:10.1016/j.cellsig.2004.12.017.
44. **Richter W**, **Menniti FS**, **Zhang HT**, **Conti M.** PDE4 as a target for cognition enhancement. *Expert Opin Ther Targets* 17: 1011–1027, 2013. doi:10.1517/14728222.2013.818656.
45. **Chabardès D**, **Montégut M**, **Zhou Y**, **Siaume-Perez S.** Two mechanisms of inhibition by prostaglandin E_2 of hormone-dependent cell cAMP in the rat collecting tubule. *Mol Cell Endocrinol* 73: 111–121, 1990. doi:10.1016/0303-7207(90)90124-q.
46. **Ishikawa S**, **Saito T.** Inhibition by phorbol ester of cellular adenosine 3',5'-monophosphate production and cellular free calcium mobilization in response to arginine vasopressin in rat renal papillary collecting tubule cells in culture. *Endocrinology* 128: 786–791, 1991. doi:10.1210/endo-128-2-786.
47. **Ecelbarger CA**, **Chou CL**, **Lolait SJ**, **Knepper MA**, **DiGiovanni SR.** Evidence for dual signaling pathways for V2 vasopressin receptor in rat inner medullary collecting duct. *Am J Physiol* 270: F623–F633, 1996. doi:10.1152/ajprenal.1996.270.4.F623.
48. **Chou CL**, **Yip KP**, **Michea L**, **Kador K**, **Ferraris JD**, **Wade JB**, **Knepper MA.** Regulation of aquaporin-2 trafficking by vasopressin in the renal collecting duct. Roles of ryanodine-sensitive Ca^{2+} stores and calmodulin. *J Biol Chem* 275: 36839–36846, 2000. doi:10.1074/jbc.M005552200.
49. **Chou CL**, **Rapko SI**, **Knepper MA.** Phosphoinositide signaling in rat inner medullary collecting duct. *Am J Physiol* 274: F564–F572, 1998. doi:10.1152/ajprenal.1998.274.3.F564.
50. **Perucca J**, **Bichet DG**, **Bardoux P**, **Bouby N**, **Bankir L.** Sodium excretion in response to vasopressin and selective vasopressin receptor antagonists. *J Am Soc Nephrol* 19: 1721–1731, 2008. doi:10.1681/ASN.2008010021.
51. **Kutina AV**, **Marina AS**, **Natochin YV.** The involvement of V1b-subtype vasopressin receptors in regulation of potassium ions excretion in the rat kidneys. *Dokl Biol Sci* 459: 338–340, 2014. doi:10.1134/S001249661406009X.
52. **Golosova DV**, **Karavashkina TA**, **Kutina AV**, **Marina AS**, **Natochin YV.** Effects of selective agonists of V1a, V2, and V1b receptors on sodium transport in rat kidney. *Bull Exp Biol Med* 160: 751–754, 2016. doi:10.1007/s10517-016-3301-x.
53. **Pena A**, **Murat B**, **Trueba M**, **Ventura MA**, **Bertrand G**, **Cheng LL**, **Stoev S**, **Szeto HH**, **Wo N**, **Brossard G**, **Serradeil-Le Gal C**, **Manning M**, **Guillon G.** Pharmacological and physiological characterization of d[Leu4, Lys8]vasopressin, the first V1b-selective agonist for rat vasopressin/oxytocin receptors. *Endocrinology* 148: 4136–4146, 2007. doi:10.1210/en.2006-1633.
54. **Grazzini E**, **Boccara G**, **Joubert D**, **Trueba M**, **Durroux T**, **Guillon G**, **Gallo-Payet N**, **Chouinard L**, **Payet MD**, **Serradeil Le Gal C.** Vasopressin regulates adrenal functions by acting through different vasopressin receptor subtypes. *Adv Exp Med Biol* 449: 325–334, 1998. doi:10.1007/978-1-4615-4871-3_41.

55. **Johnson RF**, **Beltz TG**, **Johnson AK**, **Thunhorst RL.** Effects of fludrocortisone on water and sodium intake of C57BL/6 mice. *Am J Physiol Regul Integr Comp Physiol* 309: R247–R254, 2015. doi:10.1152/ajpregu.00033.2015.
56. **Carmosino M**, **Brooks HL**, **Cai Q**, **Davis LS**, **Opalenik S**, **Hao C**, **Breyer MD.** Axial heterogeneity of vasopressin-receptor subtypes along the human and mouse collecting duct. *Am J Physiol Renal Physiol* 292: F351–F360, 2007. doi:10.1152/ajprenal.00049.2006.
57. **Wargent ET**, **Burgess WJ**, **Laycock JF**, **Balment RJ.** Separate receptors mediate oxytocin and vasopressin stimulation of cAMP in rat inner medullary collecting duct cells. *Exp Physiol* 84: 17–25, 1999. doi:10.1111/j.1469-445X.1999.tb00068.x.